Parallaxes of Southern Extremely Cool objects III: 118 L and T dwarfs

R. L. Smart [1]★ B. Bucciarelli,[1] H. R. A. Jones,[2] F. Marocco,[3] A. H. Andrei,[4]
B. Goldman,[5] R. A. Mendez,[6] V. A. d'Avila,[4] B. Burningham [2] J. I. B. Camargo,[4]
M. T. Crosta,[1] M. Daprà,[7] J. S. Jenkins,[6] R. Lachaume,[5,8] M. G. Lattanzi,[1] J. L. Penna,[4]
D. J. Pinfield,[2] D. N. da Silva Neto,[4] A. Sozzetti[1] and A. Vecchiato[1]

[1]*Istituto Nazionale di Astrofisica, Osservatorio Astrofisico di Torino, Strada Osservatorio 20, I-10025 Pino Torinese, Italy*
[2]*Center for Astrophysics Research, University of Hertfordshire, Hatfield AL10 9AB, UK*
[3]*Jet Propulsion Laboratory, California Institute of Technology, 4800 Oak Grove Dr., Pasadena, CA 91109, USA*
[4]*Observatório Nacional/MCT,R, Gal. José Cristino 77, CEP20921-400, RJ, Brazil*
[5]*Max Planck Institute for Astronomy, Koenigstuhl 17, D–69117 Heidelberg, Germany*
[6]*Departamento de Astronomia, Universidad de Chile, Casilla 36-D, Santiago, Chile*
[7]*Department of Physics and Astronomy, LaserLaB, Vrije Universiteit, De Boelelaan 1081, NL-1081 HV Amsterdam, the Netherlands*
[8]*Centro de Astroingeniería, Instituto de Astrofísica, Pontificia Universidad Católica de Chile, Vicuña Mackenna 4860, Macul, Santiago, Chile*

ABSTRACT

We present new results from the Parallaxes of Southern Extremely Cool dwarfs program to measure parallaxes, proper motions and multiepoch photometry of L and early T dwarfs. The observations were made on 108 nights over the course of 8 yr using the Wide Field Imager on the ESO 2.2m telescope. We present 118 new parallaxes of L and T dwarfs of which 52 have no published values and 24 of the 66 published values are preliminary estimates from this program. The parallax precision varies from 1.0 to 15.5 mas with a median of 3.8 mas. We find evidence for two objects with long term photometric variation and 24 new moving group candidates. We cross-match our sample to published photometric catalogues and find standard magnitudes in up to 16 pass-bands from which we build spectral energy distributions and H–R diagrams. This allows us to confirm the theoretically anticipated minimum in radius between stars and brown dwarfs across the hydrogen burning minimum mass. We find the minimum occurs between L2 and L6 and verify the predicted steep dependence of radius in the hydrogen burning regime and the gentle rise into the degenerate brown dwarf regime. We find a relatively young age of $\sim$2 Gyr from the kinematics of our sample.

Key words: parallaxes – proper motions – brown dwarfs – stars: low-mass.

1 INTRODUCTION

Objects with spectral types L and T cover the mass range from the lowest mass hydrogen burning stars, through slowly cooling sub-stellar objects down to massive Jupiter type objects. Since the first tentative discoveries 30 yr ago (Becklin & Zuckerman 1988; Latham et al. 1989) over 3000 are known today and this number will increase exponentially with the planned deep optical and infrared surveys (e.g. with the Large Synoptic Survey Telescope – LSST Science Collaboration et al. 2017; the Panoramic Survey Telescope and Rapid Response System – Chambers et al. 2016; the Wide Field Infrared Survey Telescope – Spergel et al. 2015; and Euclid – Laureijs et al. 2010). Observations and statistical studies of these objects can be used to constrain proposed stellar/sub-stellar formation processes, local galactic kinematics, understanding giant planet atmospheres, and mapping the stellar to sub-stellar boundary. The lower mass sub-stellar objects are continually cooling and therefore changing with time which, combined with their ubiquity, make them promising galactic chronometers. To realize their promise, a large sample with measured distances is needed to enable a complete calibration.

The Parallaxes of Southern Extremely Cool dwarfs (hereafter PARSEC) program was instigated to generate a large sample of these objects with measured parallaxes. In 2007, only 41 L0 to T8 objects had published parallaxes, and in PARSEC we aimed to increase the sample of objects to at least 10 for each L dwarf spectral sub-type, and, included bright southern T dwarfs to increment the T dwarf coverage. In this contribution, we report the PARSEC parallaxes of 118 L0 to T8 dwarfs which, combined with objects with literature parallaxes (described in Section 3), brings the total
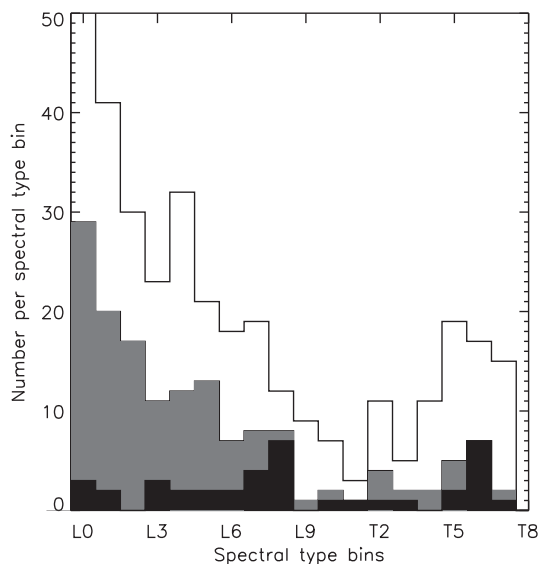
★ E-mail: richard.smart@inaf.it

Figure 1. Distribution of parallaxes of L0 to T8 dwarfs with spectral type. The black area represents the 41 objects published before 2007, the grey area the 118 PARSEC objects and the white area represents all objects published today, a total of 356 L0 to T8 objects. There is an overlap of 66 objects between the PARSEC and published objects as discussed in Section 3.1.

to 356 objects distributed in spectral type as shown in Fig. 1, which we refer to as the Full Sample.

For each L dwarf sub-type the number of objects is now at least 10, except L9 where we have 9. As discussed in Section 6, the ESA *Gaia* mission, that is measuring parallaxes for 10^9 objects, will provide a significant numbers of early L dwarfs but will have only a few late L dwarfs and less than 10 T dwarfs, so the cooler objects will remain the domain of small field pointed programs. In 2010, a complementary program to PARSEC was started on the ESO New Technology Telescope targeting late T dwarfs (Smart et al. 2013) that are too faint for PARSEC or *Gaia*.

Preliminary results for the PARSEC program have been published in Andrei et al. (2011) and Marocco et al. (2013) using observations from the first 2–3 yr; here we provide results from the full program with observations covering 8 yr. In Section 2, we briefly present the PARSEC program, in Section 3 we present the astrometric results and in Sections 4 and 5 we present applications of these results combined with literature measures to the problem of absolute magnitude calibration, local kinematics, and the location of the stellar–brown dwarf boundary.

2 THE PARSEC PROGRAM

The instrument, observational procedures, reduction procedures, and target selection is described in detail in Andrei et al. (2011), here we briefly summarize the main points.

2.1 Telescope and detector

The PARSEC observations were made on the Wide Field Imager (WFI; Baade et al. 1999) of the ESO MPIA 2.2m telescope. This is a mosaic of 8 EEV CCD44 chips with 2k×4k 15 μm pixels, for the results presented here we only used observations from the top half of CCD#7 (Priscilla). Limiting our reductions to this region was a balance between simplicity of the required astrometric transforms – the larger the adopted area being modelled the more complicated

transforms were required – and number of anonymous reference stars for which we required a minimum of 12.

This telescope and instrument combination has a number of positive characteristics:

(i) The camera is fixed and stable, crucial for small field relative astrometry.

(ii) The 0.2 arcsec pixel^{-1} focal plane scale allows at least 2 pixels per full width at half-maximum (e.g. Nyquist sampling) even in the best seeing.

(iii) The total field size of 0.3 deg provides a large field to search for nearby companions.

(iv) This combination had already been used for the determination of parallaxes (Ducourant et al. 2007).

We observed all objects in the z band (Z+/61 ESO#846, central wavelength 964.8 μm, FWHM 61.6 μm) which provided the best ratio of exposure time and signal to noise for these very red targets.

2.2 Observational procedure

Each observation consisted of a short exposure to visually locate the target and then an application of the WFI move-to-pixel procedure to move the target to pixel 3400, 3500 in CCD#7. We then made two exposures of 150 s for objects with $z \leq 18.0$ and 300 s for $z \geq 18.0$ offset by 24 pixels in both axes. If we found the signal to noise of the first exposure to be less than 100 we increased the exposure time of the second accordingly. The short location frames were saved and used in the reduction process to model the z-band fringing.

To minimize differential reddening corrections (Monet et al. 1992), we attempt to observe all targets within 30 min of the meridian. The total time for each target is 10–25 min which enable an average of 3–4 targets h^{-1}. Our observing runs were usually allocated in blocks of 3 nights spread throughout the year. Observations began on 2007 April 9 and using nights obtained via Brazilian and ESO allocations continued for 4 yr until 2011 July 21. After this date, this telescope was no longer available through ESO or Brazil and we obtained three additional runs in 2014 March, 2015 October, and 2016 February from the CNTAC, OPTICON and a few service observations on MPIA time. In these extra runs, we were able to re-observe most targets extending the coverage to over 8 yr providing important leverage to separate parallax and proper motion components.

2.3 Target selection

The target lists had to meet a number of practical and scientific considerations. The combination of a variable time allocation and the requirement of observing objects close to the meridian required us to have a target list that covered the whole 24 h right ascension range uniformly. To give flexibility for matching targets to conditions, and, to ensure that any target was only observed in 2 out of each 3 night run, we built redundancy into the list. With these requirements in mind, we adopted the following criteria:

(i) Southern ($\delta < 0°$) confirmed L and T dwarfs discovered before 2007 April,

(ii) Magnitude in the z band brighter than 19,

(iii) Between 6 and 8 objects in any RA hour,

(iv) The brightest examples within each spectral bin,

(v) A uniform spectral class distribution for L dwarfs,

(vi) A photometric distance smaller than 50 pc.

The photometric distances were estimated using the Two Micron All-Sky Survey (2MASS; Skrutskie et al. 2006) magnitudes transformed to the MKO system using Stephens & Leggett (2004) and the colour – absolute magnitude compilation given in Knapp et al. (2004). This produced an original target list of 140 targets that can be found in Andrei et al. (2011).

In Table 1, we list the 118 targets published here including a short name for each object used throughout this paper, the discovery name, the z-band magnitude adopted at the beginning of the program and, when they exist, published values of optical/NIR spectral types, radial velocities, and parallaxes. The last column summarizes any published indications of multiplicity, e.g. if the object is an unresolved binary (at the nominal WFI resolution), in a wide binary system or a moving group candidate. The distribution of the 118 targets is shown in Fig. 1 with respect to all L0 to T2 objects with published parallaxes.

2.4 Image reduction procedure

All images were bias corrected and flat fielded using standard *IRAF CCDPROC* procedures. The WFI z-band images have strong interference fringes that were removed using *RMFRINGE* with a fringe

Table 1. Targets, published magnitudes, spectral types, radial velocities, and parallaxes.

Target code	Discovery name[Ref.]	z band mag	Optical. SpT[Ref.]	NIR SpT[Ref.]	RV, σ_{RV}[Ref.] km s^{-1}	ϖ, σ_ϖ[Ref.] mas	Multiple code[Ref.]
0004-4044	GJ1001B[2]	15.8	L5[14]	L4.5[39]	32.9, 0.2[71]	77.0, 2.1[83]	VB;[40]
0013-2235	2MASSIJ0013578-223520[27]	18.6	L4[27]	L5.5[85]	–	–	
0016-4056	2MASS00165953-4056541[63]	18.0	L3.5[63]	–	–	–	
0032-4405	EROS-MPJ0032-4405[2]	17.1	L0γ[65]	L0γ[77]	–	38.4, 4.8[74]	MG;[84]
0034-0706	2MASSIJ0034568-070601[27]	18.2	L3[27]	L4.5[85]	–	–	
0054-0031	SDSSpJ005406.55-003101.8[18]	18.3	L1[19]	L2[85]	−5.7, 13.0[69]	–	
0058-0651	2MASSWJ0058425-065123[9]	17.1	L0[9]	L0[85]	–	33.8, 4.0[76]	MG;[84]
0109-5100	2MASS01090150-5100494[17]	14.6	M8.5[44]	L2[44]–	–	57.8, 3.3[76]	
0117-3403	2MASSIJ0117474-340325[31]	17.9	L2:[31]	L1β[77]	–	26.1, 1.9	MG;[84]
0128-5545	2MASS01282664-5545343[54]	16.6	L2[60]	L1[54]	–	–	
0144-0716	2MASS01443536-0716142[28]	16.9	L5[28]	L5[76]	−2.6, 0.1[71]	–	
0147-4954	2MASSJ01473282-4954478[49]	15.8	–	L2.0[76]–	–	–	
0205-1159	DENIS-PJ0205.4-1159[1]	17.4	L7[5]	L5.5[39]	–	54.3, 1.6[88]	UR;[45]
0219-1938	SSSPMJ0219-1939[17]	16.9	L1[44]	L2.5[44]	–	37.2, 4.1[76]	
0227-1624	2MASS02271036-1624479[60]	16.1	L1[60]	L0.5:[76]	48.5, 0.2[71]–	–	
0230-0953	DENISJ02304500-0953050[68]	17.7	L0[68]	L1[85]	–	32.4, 3.7[76]	
0235-0849	2MASS02354756-0849198[19]	18.3	L2[19]	L2:[85]	22.8, 6.1[69]	–	
0235-2331	GJ1048B[13]	15.2	L1[13]	L1[13]	15.4, 0.1[71]	47.0, 0.9[55]	VB;[13]
0239-1735	2MASSIJ0239424-173547[31]	16.6	L0[31]	M9[76]–	–	32.1, 4.7[76]	
0255-4700	DENIS-PJ0255-4700[4]	16.1	L8[63]	L9[51]	–	205.8, 0.5[88]	
0257-3105	2MASS02572581-3105523[63]	17.6	L8[63]	L8:[76]	–	99.7, 6.7[76]	
0318-3421	2MASS03185403-3421292[63]	18.5	L7[63]	–	–	72.9, 7.7[74]	
0357-0641	2MASS03572110-0641260[19]	18.3	L0[19]	–	89.7, 41.1[59; 69]	–	
0357-4417	DENIS-PJ035726.9-441730[30]	16.7	L0β[63]	L2p[76]	–	–	MG;[84]
0408-1450	2MASSIJ0408290-145033[35]	16.9	L2[31]	L4.5[35]	–	–	
0423-0414	SDSSpJ042348.57-041403.5[22]	17.3	L7.5[31]	T0[51]	–	67.5, 2.3[88]	UR;[51]
0439-2353	2MASSIJ0439010-235308[31]	17.3	L6.5[31]	L4.5[82]	–	110.4, 4.0[74]	
0518-2828	2MASS05185995-2828372[41]	18.8	L7[63]	L6+T4[53]	–	43.7, 0.8[75]	UR;[41; 53]
0523-1403	2MASSIJ0523382-140302[31]	15.9	L2.5[31]	L5[35]	12.2, 0.1[71]	80.9, 1.8[83]	
0539-0059	SDSSpJ053951.99-005902.0[8]	16.7	L5[8]	L5[39]	13.9, 0.2[71]	79.2, 1.0[88]	
0559-1404	2MASS05591914-1404488[10]	17.3	T5[32]	T4.5[51]	–	96.8, 1.2[88]	
0614-2019	SIPSJ0614-2019[73]	17.6	–	L4[73]	–	34.3, 3.0[76]	
0624-4521	2MASS06244595-4521548[60]	17.2	L5:[60]	L5[85]	–	81.2, 0.4[88]	
0639-7418	2MASS06395596-7418446[56]	18.5	L5[56]	–	–	–	
0641-4322	2MASS06411840-4322329[60]	16.3	L1.5[60]	L2.5:[85]	–	51.1, 0.5[88]	
0719-5051	2MASS07193188-5051410[60]	16.5	L0[60]	L0:[76]	–	34.6, 2.2[76]	
0729-7843	2MASSJ07291084-7843358[73]	18.3	–	L0.0[76]	–	–	
0828-1309	SSSPMJ0829-1309[24]	15.6	L2[44]	L2:[76]	25.8, 0.1[71]	85.8, 0.1[81]	
0832-0128	2MASSWJ0832045-012835[9]	16.6	L1.5[9]	L1[85]	20.0, 1.3[26]	40.4, 1.8[88]	
0835-0819	2MASSIJ0835425-081923[31]	15.9	L5[31]	L4[76]	–	137.5, 0.4[88]	
0859-1949	2MASSIJ0859254-194926[31]	18.4	L6:[31]	L8[80]	–	65.4, 6.1[74]	
0909-0658	DENIS-PJ0909-0658[3]	16.2	L0[63]	L0[85]	–	42.5, 4.2[73]	
0921-2104	2MASS09211410-2104446[60]	15.5	L1.5[60]	L4p(blue)[61]	–	–	
0922-8010	2MASS09221952-8010399[60]	18.1	L2:[60]	–	–	–	
0928-1603	2MASSWJ0928397-160312[9]	18.1	L2[9]	L2:[76]	–	34.4, 3.9[76]	
1004-1318	DENISJ1004403-131818[68]	17.6	L0[68]	L1:[76]	–	–	
1004-3335	2MASSWJ1004392-333518[23]	17.3	L4[23]	L4.5[85]	–	54.8, 5.6[73]	VB;[47]
1018-2909	2MASSWJ1018588-290953[23]	16.7	L1[23]	L0.5[85]	–	35.3, 3.2[73]	
1045-0149	2MASSIJ1045240-014957[23]	15.7	L1[23]	L2[76]	–	61.8, 1.5	MG;[64]

Table 1 *– continued*

Target code	Discovery name[Ref.]	z band mag	Optical. SpT[Ref.]	NIR SpT[Ref.]	RV, σ_{RV}[Ref.] km s^{-1}	ϖ, σ_ϖ[Ref.] mas	Multiple code[Ref.]
1047-1815	DENIS-PJ1047-1815[4]	17.0	L2.5[4]	L0.5[85]	–	37.9, 1.9	
1058-1548	DENIS-PJ1058.7-1548[1]	16.9	L3[5]	L3[39]	–	55.9, 0.6[88]	MG;[86]
1059-2113	2MASSIJ1059513-211308[31]	17.1	L1[31]	L3:[85]	–	–	
1122-3512	2MASS11220826-3512363[46]	18.1	–	T2[51]	–	–	
1122-3916	2MASSWJ1122362-391605[23]	18.4	L3[23]	L3.5:[85]	–	–	
1126-5003	2MASS11263991-5003550[58]	15.9	L4.5[61]	L6.5p[61]	–	60.8, 2.0[88]	
1154-3400	2MASS11544223-3400390[30]	16.6	L0[63]	L0.5[85]	–	–	MG;[87]
1225-2739	2MASS12255432-2739466[6]	18.8	T6[32]	T6[51]	–	75.1, 2.5[29]	UR;[33]
1228-1547	DENIS-PJ1228.2-1547[1]	17.2	L5[5]	L6[39]	19.4, 5.0[72]	44.8, 1.8[75]	UR;[30]
1246-3139	WISEJ124629.65-313934.2[73]	18.2	–	T2:[78]	–	87.3, 3.2[76]	
1254-0122	SDSSpJ125453.90-012247.4[12]	18.0	T2[32]	T2[51]	–	84.9, 1.9[20]	
1326-2729	2MASSWJ1326201-272937[23]	18.6	L5[23]	L6.5:[85]	–	–	MG;[87]
1331-0116	2MASS13314894-0116500[19]	18.4	L6[19]	L8p(blue)[39]	–	67.3, 12.6[76]	
1341-3052	2MASS13411160-3052505[60]	17.3	L2:[60]	L2.5:[85]	33.7, 5.0[72]	–	SB;[85]
1404-3159	2MASS14044948-3159330[57]	18.8	T0[62]	T2.5[57]	–	42.1, 1.1[75]	UR;[62]
1425-3650	DENIS-PJ142527.97-365023.4[36]	16.5	L3:[60]	L5[36]	5.3, 0.3[71]	86.4, 0.8[83]	MG;[86]
1438-1309	2MASSWJ1438549-130910[9]	18.2	L3:[9]	L3[85]	–	–	
1441-0945	G124-62BC[4]	16.4	L0.5[63]	L0.5[85]	–	30.7, 0.7[88]	VB;[30; 43]
1457-2121	Gliese570D[11]	18.8	T7[32]	T7.5[51]	–	167.6, 4.6[88]	VB;[11]
1507-1627	2MASSWJ1507476-162738[7]	15.6	L5[9]	L5.5[39]	-39.8, 0.1[71]	133.9, 0.6[88]	
1520-4422B	WDSJ15200-4423B[54]	16.0	–	L4.5[51]	–	–	
1523-2347	2MASS15230657-2347526[54]	17.0	–	L2.5[54]	–	–	
1530-8145	2MASSJ15302867-8145375[37]	17.0	–	L0.0[76]	–	–	
1534-2952	2MASSIJ1534498-295227[21]	18.4	T6[32]	T5.5[51]	–	62.4, 1.3[75]	UR;[34]
1539-0520	DENIS-PJ153941.96-052042.4[36]	16.6	L4:[63]	L2[36]	–	60.1, 1.2[88]	
1547-2423	2MASS15474719-2423493[60]	16.3	M9p[60]	L0Int-G[77]	–	30.0, 1.1	MG;[87]
1548-1636	2MASS15485834-1636018[54]	16.7	–	L2:[54]	–	–	
1618-1321	2MASS16184503-1321297[63]	16.6	L0:[63]	M9.5[85]	–	21.9, 1.3[88]	
1620-0416	GJ618.1B[15]	18.0	L2.5[15]	L2.5[85]	–	29.9, 2.7[55]	VB;[15]
1633-0640	2MASS16335933-0640552[48]	19.0	–	L6[48]	–	–	
1636-0034	SDSSpJ163600.79-003452.6[8]	17.0	L0[8]	M9[85]	−7.4, 4.1[59; 69]	–	
1645-1319	2MASSWJ1645221-131951[23]	15.0	L1.5[23]	–	–	89.3, 0.4[88]	
1705-0516	DENIS-PJ170548.38-051645.7[36]	16.1	–	L4[36]	–	53.5, 1.0	UR;[49]
1707-0558	2MASS17072343-0558249[50]	16.7	–	L3[50]	–	–	UR;MG;[50]
1750-0016	2MASS17502484-0016151[54]	16.0	–	L5.5[54]	–	108.8, 0.8[88]	
1753-6559	2MASS17534518-6559559[60]	16.9	L4:[60]	L4:[76]	–	58.0, 4.9[76]	
1828-4849	2MASS18283572-4849046[42]	18.7	–	T5.5[51]	–	87.9, 2.0[79]	
1840-5631	2MASSJ18401904-5631138[73]	18.9	–	L9.0[76]	–	–	
1928-4356	2MASS19285196-4356256[60]	17.9	L4[60]	L4p[76]	–	–	
1936-5502	2MASS19360187-5502322[60]	17.2	L5:[60]	L4[76]	–	43.3, 4.5[76]	
1956-1754	2MASS19561542-1754252[54]	16.1	M8[60]	L0:[54]	–	–	
2002-0521	2MASS20025073-0521524[56]	18.2	L6[56]	L7:[85]	–	–	
2011-6201	2MASSJ20115649-6201127[73]	18.8	–	sdM8[76]	–	–	
2023-5946	2MASSJ20232858-5946519[73]	18.7	–	M8.0[76]	–	–	
2026-2943	2MASS20261584-2943124[56]	17.3	L1:[56]	L1+T6:[70]	–	–	UR;[70; 85]
2041-3506	2MASS20414283-3506442[56]	17.6	L2:[56]	L2[85]	–	–	MG;[86]
2045-6332	SIPS2045-6332[76]	15.4	–	L1:[76]	–	41.7, 1.5[83]	MG;[72]
2057-0252	2MUCD12054[31]	15.6	L1.5[31]	L1.5[36]	−24.6, 0.4[71]	64.7, 0.8[88]	
2101-2944	2MASS21015233-2944050[76]	18.8	–	L1[76]	–	–	
2104-1037	2MASSIJ2104149-103736[31]	16.6	L2.5[63]	–	–	57.2, 0.9[88]	
2107-4544	2MASS21075409-4544064[60]	17.3	L0:[60]	L2.5[85]	–	–	
2130-0845	2MASSWJ2130446-084520[63]	16.7	L1.5[63]	M8.5[85]	–	–	
2132-1452	2MASS21324898-1452544[76]	19.0	–	T4[76]	–	–	
2150-7520	2MASS21501592-7520367[60]	16.6	L1:[60]	–	–	–	
2157-5534	2MASS21574904-5534420[60]	17.0	L0:[60]	–	–	–	
2158-1550	2MASS21580457-1550098[63]	17.8	L4:[63]	L4.5:[85]	–	–	
2204-5646	epsIndiBab[25]	16.7	–	T1+T6[51]	–	275.3, 3.0[88]	VB;[16]
2206-4217	2MASSWJ2206450-421721[9]	18.3	L2[9]	L4:[85]	–	–	
2209-2711	2MASS22092183-2711329[76]	18.9	–	T2.5[76]	–	47.9, 12.5[76]	
2213-2136	2MASS22134491-2136079[56]	17.9	L0Int-G[63]	L0Int-G[77]	–	20.9, 1.9	
2224-0158	2MASSWJ2224438-015852[9]	16.9	L4.5[9]	L3.5[39]	−37.6, 0.1[71]	86.1, 0.9[88]	
2252-1730	DENIS-PJ225210.73-173013.4[36]	17.2	–	L7.5[36]	–	63.2, 1.6[75]	UR;[52]
2254-2840	2MASSIJ2254519-284025[31]	16.5	L0.5[31]	L0.5[36]	–	–	

Table 1 – *continued*

Target code	Discovery name[Ref.]	z band mag	Optical. SpT[Ref.]	NIR SpT[Ref.]	RV, σ_{RV}[Ref.] km s^{-1}	ϖ, σ_ϖ[Ref.] mas	Multiple code[Ref.]
2255-0034	SDSSpJ225529.09-003433.4[18]	18.0	L0:[18]	M8.5[85]	12.3, 24.0[59; 69]	16.2, 2.6[38]	
2310-1759	SSSPMJ2310-1759[17]	16.9	L0:[56]	L1[44]	–	36.4, 6.9[76]	
2318-1301	2MASS23185497-1301106[76]	18.8	–	T5[76]	–	–	
2330-0347	2MASS23302258-0347189[56]	17.0	L1:[56]	L0.5[85]	–	–	
2346-5928	SIPS2346-5928[73]	17.3	–	L5.0[76]	–	–	
2351-2537	2MASS23515044-2537367[67]	14.8	L0.5[67]	–	−10.0, 3.0[66]	–	

Notes. Multiple code: VB – visual binary, UR – unresolved binary, MG – moving group, Bi – binary, SB – spectral binary References 1: Delfosse et al. (1997), 2: EROS Collaboration et al. (1999), 3: Delfosse et al. (1999), 4: Martín et al. (1999), 5: Kirkpatrick et al. (1999), 6: Burgasser et al. (1999), 7: Reid et al. (2000), 8: Fan et al. (2000), 9: Kirkpatrick et al. (2000), 10: Burgasser et al. (2000a), 11: Burgasser et al. (2000b), 12: Leggett et al. (2000), 13: Gizis, Kirkpatrick & Wilson (2001), 14: Kirkpatrick et al. (2001), 15: Wilson et al. (2001), 16: Mason et al. (2001), 17: Lodieu, Scholz & McCaughrean (2002), 18: Schneider et al. (2002), 19: Hawley et al. (2002), 20: Dahn et al. (2002), 21: Burgasser et al. (2002), 22: Geballe et al. (2002), 23: Gizis (2002), 24: Scholz & Meusinger (2002), 25: Scholz et al. (2003), 26: Guenther & Wuchterl (2003), 27: Kendall et al. (2003), 28: Liebert et al. (2003), 29: Tinney, Burgasser & Kirkpatrick (2003), 30: Bouy et al. (2003), 31: Cruz et al. (2003), 32: Burgasser, McElwain & Kirkpatrick (2003a), 33: Burgasser et al. (2003b), 34: Burgasser et al. (2003c), 35: Wilson et al. (2003), 36: Kendall et al. (2004), 37: Scholz et al. (2004), 38: Vrba et al. (2004), 39: Knapp et al. (2004), 40: Golimowski et al. (2004), 41: Cruz et al. (2004), 42: Burgasser (2004), 43: Seifahrt, Guenther & Neuhäuser (2005b), 44: Lodieu et al. (2005), 45: Bouy et al. (2005), 46: Tinney et al. (2005), 47: Seifahrt et al. (2005a), 48: Chiu et al. (2006), 49: Reid et al. (2006a), 50: McElwain & Burgasser (2006), 51: Burgasser, Burrows & Kirkpatrick (2006b), 52: Reid et al. (2006b), 53: Burgasser et al. (2006a), 54: Kendall et al. (2007), 55: van Leeuwen (2007), 56: Cruz et al. (2007), 57: Looper, Kirkpatrick & Burgasser (2007), 58: Folkes et al. (2007), 59: West et al. (2008), 60: Reid et al. (2008), 61: Burgasser et al. (2008), 62: Looper et al. (2008), 63: Kirkpatrick et al. (2008), 64: Jameson et al. (2008), 65: Cruz, Kirkpatrick & Burgasser (2009), 66: Reiners & Basri (2009), 67: Seifahrt et al. (2010), 68: Martín et al. (2010), 69: Schmidt et al. (2010), 70: Gelino & Burgasser (2010), 71: Blake, Charbonneau & White (2010), 72: Gálvez-Ortiz et al. (2010), 73: Andrei et al. (2011), 74: Faherty et al. (2012), 75: Dupuy & Liu (2012), 76: Marocco et al. (2013), 77: Allers & Liu (2013), 78: Mace et al. (2013), 79: Smart et al. (2013), 80: Thompson et al. (2013), 81: Sahlmann et al. (2014), 82: Schneider et al. (2014), 83: Dieterich et al. (2014), 84: Gagné et al. (2014), 85: Bardalez Gagliuffi et al. (2014), 86: Gagné et al. (2015b), 87: Gagné et al. (2015a), 88: Weinberger et al. (2016).

map made with three steps: (1) mask out all objects in all short exposures and four of the long exposures; (2) make a median image of the unmasked pixels scaling all images by the exposure time; and (3) smooth the median image using a 5 pixel box car average. After subtracting this fringe map scaled by the exposure time from the cleaned images, we again make a new fringe map and again subtract it, this time scaled by the mean sky count. We did not use all the long exposures in the construction of the fringe map as the move-target-to-pixel and masking procedures are not perfect so the resultant fringe map using all frames often had a halo around the target position. The telescope pointing is only good to a few arcseconds so in the location frames the target is rarely in the same position and this halo problem does not occur.

In Andrei et al. (2011), we adopted the Torino Observatory Parallax Program (TOPP; Smart et al. 1999) centroiding procedures but, as discussed in Marocco et al. (2013), we found the Cambridge Astronomy Survey Unit's *imcore* maximum likelihood barycentre (CASUTOOLS, v 1.0.21) more consistent so we have adopted that package to determine the centroids of all objects in the field.

2.5 Astrometric parameter determination

The astrometric reduction was carried out using TOPP pipeline procedures and the reader is referred to Smart et al. (1999) for details, here we just outline the main steps. A base frame, observed on a night with good seeing, was selected and the measured *x*, *y* positions of all objects were transformed to a standard coordinate ξ, η system determined from a gnomic projection of the *Gaia* DR1 objects in the frame. All subsequent frames were transformed to this standard coordinate system with a simple six constant linear astrometric fit using all common objects except the target. We then removed any frames that had an average reference star error larger than the mean error for all frames plus three standard deviations about that mean in either coordinate, or, had less than 12 stars in common with the base frame.

Since the target is not used in the fit, its positional change is a reflection of its parallax and proper motion. We fit a simple 5 parameter model to this positional change, and that of all the other objects in the field, to find their astrometric parameters implicitly assuming all objects are single. We then iterate this procedure where, in addition to removing frames as described above, we also remove stars with large errors over the sequence from the objects used to astrometrically transform frames. Finally, for the target solution we removed any observations where the combined residual in the two coordinates is greater than three times the σ of the whole solution.

The solutions were tested for robustness using bootstrap-like testing where we iterate through the sequence selecting different frames as the base frame thus making many solutions that incorporate varied sets of reference stars and starting from different dates. We create the subset of all solutions with: (i) a parallax within one σ of the median solution; (ii) the number of included observations in the top 10 per cent; and (iii) at least 12 reference stars in common to all frames. From this subset, for this publication, we have selected the one with the smallest error. More than 90 per cent of the solutions were within one σ of the published solution.

To the relative parallaxes, we add a correction (COR in Table 2) to find astrophysically useful absolute parallaxes. The COR is estimated from the average magnitude of the common reference stars and the Galaxy model of Mendez & van Altena (1996) in the *z* band. When *Gaia* produces proper motions and parallaxes of the anonymous field objects, we will be able to tie more precisely to the absolute system.

3 ASTROMETRIC RESULTS

In Table 2, we present the astrometric results for the 118 targets, listed are positions at epoch 2010, epoch of the base frame, parallaxes, proper motions, relative to absolute corrections applied

Table 2. Astrometric parameters of PARSEC targets.

Target	$\alpha\ \delta$ deg epoch 2010	Baseframe epoch	$\varpi_{abs} \pm \sigma$ mas	$\mu_\alpha \cos\delta \pm \sigma$ mas yr^{-1}	$\mu_\delta \pm \sigma$ mas yr^{-1}	COR mas	$N_*, N_o, \Delta T$ yr
0004-4044	1.1477475, − 40.7392975	2009.56	77.48 ± 4.64	668.67 ± 1.30	− 11498.18 ± 1.29	0.55	6, 26, 8.10
0013-2235	3.4910061, − 22.5891701	2009.73	46.83 ± 11.55	60.45 ± 6.66	− 69.37 ± 11.22	0.44	8, 9, 3.21
0016-4056	4.2488780, − 40.9482895	2007.77	44.68 ± 11.39	196.06 ± 5.37	24.92 ± 6.54	0.62	8, 5, 1.97
0032-4405	8.2331843, − 44.0852233	2010.86	29.30 ± 4.72	120.68 ± 1.30	− 95.88 ± 1.38	0.52	10, 26, 8.00
0034-0706	8.7374725, − 7.1008713	2009.97	55.83 ± 12.26	197.07 ± 9.04	− 160.68 ± 6.22	− 0.14	5, 12, 3.11
0054-0031	13.5279543, − 0.5177292	2010.63	12.65 ± 4.87	192.24 ± 1.27	− 157.02 ± 1.64	0.69	10, 18, 8.11
0058-0651	14.6777007, − 6.8570328	2008.64	32.95 ± 4.77	143.15 ± 1.01	− 123.22 ± 0.86	0.46	9, 30, 8.10
0109-5100	17.2573429, − 51.0135480	2009.56	62.52 ± 2.63	219.42 ± 0.86	75.71 ± 0.69	0.46	10, 29, 8.10
0117-3403	19.4482615, − 34.0573392	2009.72	19.81 ± 6.04	93.36 ± 1.58	− 45.84 ± 2.17	0.25	6, 16, 8.09
0128-5545	22.1098342, − 55.7592488	2007.67	50.24 ± 5.96	− 248.50 ± 1.53	118.85 ± 2.31	0.24	9, 24, 8.10
0144-0716	26.1484149, − 7.2712842	2009.97	74.23 ± 5.16	377.71 ± 1.15	− 187.14 ± 1.39	0.11	8, 5, 8.10
0147-4954	26.8864692, − 49.9140583	2009.96	25.54 ± 2.99	− 59.83 ± 0.90	− 265.91 ± 0.70	0.63	9, 24, 8.09
0205-1159	31.3736178, − 11.9914857	2009.96	54.09 ± 3.90	429.44 ± 0.93	52.87 ± 0.89	0.45	10, 25, 8.10
0219-1938	34.8675775, − 19.6452902	2010.86	32.62 ± 4.92	182.41 ± 1.76	− 98.63 ± 1.74	0.31	7, 13, 7.75
0227-1624	36.7943950, − 16.4141398	2009.73	54.22 ± 4.44	429.97 ± 1.42	− 300.66 ± 1.16	0.37	7, 19, 8.09
0230-0953	37.6879324, − 9.8849150	2007.67	30.44 ± 2.78	150.08 ± 0.65	− 63.40 ± 1.36	0.68	5, 24, 8.10
0235-0849	38.9481393, − 8.8221609	2009.73	30.10 ± 2.56	− 50.62 ± 1.79	17.37 ± 13.16	0.21	6, 7, 2.98
0235-2331	39.0000280, − 23.5222961	2009.96	41.73 ± 7.41	95.03 ± 4.81	38.91 ± 10.53	1.07	8, 12, 2.97
0239-1735	39.9274815, − 17.5961006	2008.82	29.71 ± 2.93	55.57 ± 0.67	− 93.75 ± 0.73	0.53	6, 22, 8.10
0255-4700	43.7695401, − 47.0158453	2010.63	206.06 ± 5.81	1012.52 ± 2.13	− 550.88 ± 2.93	0.30	6, 15, 7.99
0257-3105	44.3597881, − 31.0968375	2010.64	101.60 ± 6.68	605.88 ± 1.49	339.17 ± 1.82	0.74	9, 12, 6.80
0318-3421	49.7266300, − 34.3580202	2009.73	44.67 ± 15.60	392.91 ± 2.86	47.07 ± 2.89	0.36	8, 5, 6.81
0357-0641	59.3404787, − 6.6904842	2010.65	10.70 ± 4.14	140.54 ± 0.83	10.90 ± 0.96	0.39	11, 26, 8.10
0357-4417	59.3626437, − 44.2918283	2010.64	16.77 ± 2.99	64.18 ± 0.60	− 9.57 ± 0.99	0.38	11, 25, 8.10
0408-1450	62.1202147, − 14.8429450	2010.98	46.88 ± 3.33	199.95 ± 0.80	− 97.45 ± 1.06	0.55	9, 29, 8.10
0423-0414	65.9515200, − 4.2340809	2008.96	71.97 ± 3.23	− 322.98 ± 0.80	85.43 ± 1.06	0.58	8, 27, 8.01
0439-2353	69.7642946, − 23.8867150	2011.13	82.72 ± 4.03	− 112.81 ± 1.14	− 155.28 ± 0.95	0.49	16, 35, 8.01
0518-2828	79.7496314, − 28.4778602	2010.87	44.61 ± 5.08	− 75.57 ± 1.32	− 269.53 ± 2.01	0.54	17, 26, 8.41
0523-1403	80.9095684, − 14.0501604	2015.77	79.44 ± 2.12	105.05 ± 0.61	164.79 ± 1.02	0.54	18, 36, 8.02
0539-0059	84.9670678, − 0.9828936	2010.98	79.89 ± 1.33	161.03 ± 0.37	323.12 ± 0.42	0.57	23, 39, 8.40
0559-1404	89.8315807, − 14.0813086	2009.96	97.88 ± 1.78	570.52 ± 0.51	− 339.63 ± 0.69	0.58	28, 39, 8.02
0614-2019	93.5502757, − 20.3226490	2011.13	35.32 ± 2.23	140.92 ± 0.79	− 308.66 ± 0.49	0.59	40, 45, 8.40
0624-4521	96.1918822, − 45.3641483	2009.73	82.16 ± 1.88	− 34.18 ± 0.62	368.76 ± 0.93	0.59	8, 33, 8.02
0639-7418	99.9833256, − 74.3123259	2010.86	50.78 ± 7.54	18.36 ± 2.25	0.93 ± 2.33	0.58	16, 32, 8.89
0641-4322	100.3275249, − 43.3740297	2010.98	50.72 ± 1.18	211.86 ± 0.38	625.75 ± 0.60	0.58	30, 40, 8.41
0719-5051	109.8835887, − 50.8615515	2011.23	33.35 ± 1.42	174.36 ± 0.42	− 50.70 ± 0.68	0.56	23, 47, 8.90
0729-7843	112.2928751, − 78.7261905	2010.97	10.07 ± 2.75	− 152.88 ± 0.92	137.06 ± 1.13	0.54	28, 48, 8.89
0828-1309	127.1413758, − 13.1564006	2010.87	84.24 ± 1.40	− 569.63 ± 0.37	4.47 ± 0.49	0.60	20, 43, 8.90
0832-0128	128.0192365, − 1.4766709	2010.98	42.57 ± 1.90	64.72 ± 0.50	11.55 ± 0.63	0.59	13, 46, 8.16
0835-0819	128.9229611, − 8.3219362	2008.97	146.19 ± 2.82	− 559.34 ± 0.66	309.40 ± 0.47	0.60	32, 35, 8.90
0859-1949	134.8551364, − 19.8244429	2011.21	71.22 ± 3.54	− 323.03 ± 0.76	− 97.72 ± 0.68	0.57	37, 39, 8.89
0909-0658	137.4890435, − 6.9720179	2009.23	35.99 ± 2.19	− 184.43 ± 0.61	20.19 ± 0.52	0.55	17, 39, 8.90
0921-2104	140.3094109, − 21.0816119	2011.21	77.87 ± 1.60	254.13 ± 0.35	− 915.10 ± 0.45	0.56	18, 38, 8.90
0922-8010	140.5818017, − 80.1766907	2009.24	40.29 ± 4.35	39.40 ± 1.19	− 55.85 ± 1.57	0.53	31, 34, 8.89
0928-1603	142.1649531, − 16.0534848	2008.26	32.38 ± 2.78	− 157.34 ± 0.59	26.36 ± 0.72	0.56	20, 38, 8.90
1004-1318	151.1675640, − 13.3058472	2009.96	37.89 ± 1.92	− 121.80 ± 0.50	− 190.37 ± 0.55	0.48	13, 44, 8.90
1004-3335	151.1625165, − 33.5869592	2014.22	45.80 ± 2.87	343.58 ± 0.58	− 345.45 ± 0.67	0.56	45, 31, 8.90
1018-2909	154.7438393, − 29.1651446	2014.22	33.86 ± 1.43	− 342.53 ± 0.37	− 92.23 ± 0.69	0.57	20, 40, 8.90
1045-0149	161.3485657, − 1.8323859	2009.17	52.41 ± 3.21	− 488.66 ± 0.70	− 5.73 ± 0.66	0.47	10, 29, 8.90
1047-1815	161.8783338, − 18.2658328	2009.35	31.49 ± 4.24	− 352.60 ± 0.80	43.65 ± 0.63	0.57	12, 32, 8.89
1058-1548	164.6985694, − 15.8047221	2009.17	49.22 ± 3.11	− 255.34 ± 0.70	37.94 ± 0.71	0.50	10, 38, 8.89
1059-2113	164.9644957, − 21.2195072	2010.32	28.29 ± 2.95	107.30 ± 0.65	− 160.43 ± 0.65	0.40	12, 36, 8.89
1122-3512	170.5339242, − 35.2109038	2011.12	78.61 ± 5.96	− 131.73 ± 0.65	− 263.52 ± 1.34	0.60	22, 26, 8.01
1122-3916	170.6511768, − 39.2687366	2014.21	32.49 ± 7.62	49.75 ± 1.11	− 184.43 ± 1.02	0.57	53, 26, 8.01
1126-5003	171.6589674, − 50.0640251	2011.21	63.23 ± 1.95	− 1583.13 ± 0.56	454.42 ± 0.40	0.42	66, 34, 7.92
1154-3400	178.6753759, − 34.0108286	2011.21	30.15 ± 3.16	− 156.78 ± 0.65	17.23 ± 0.61	0.51	26, 35, 8.01
1225-2739	186.4777455, − 27.6649768	2011.12	78.96 ± 11.41	374.84 ± 1.33	− 624.75 ± 1.38	0.33	25, 21, 8.01
1228-1547	187.0638399, − 15.7934534	2009.57	45.78 ± 2.97	130.83 ± 0.52	− 179.44 ± 1.13	0.50	15, 31, 8.01
1246-3139	191.6235015, − 31.6594760	2009.37	88.38 ± 3.43	− 5.24 ± 0.61	− 560.84 ± 0.96	0.39	37, 31, 8.01
1254-0122	193.7232580, − 1.3796031	2010.46	68.04 ± 6.53	− 476.70 ± 1.11	120.42 ± 0.86	0.40	5, 28, 8.01
1326-2729	201.5825064, − 27.4937769	2014.22	39.80 ± 8.66	− 362.07 ± 1.22	− 24.19 ± 1.11	0.39	28, 25, 8.01
1331-0116	202.9526675, − 1.2837683	2016.17	49.98 ± 4.59	− 406.62 ± 0.98	− 1035.16 ± 1.54	0.26	8, 15, 7.91

Table 2 – *continued*

Target	α δ deg epoch 2010	Baseframe epoch	$\varpi_{abs} \pm \sigma$ mas	$\mu_\alpha \cos\delta \pm \sigma$ mas yr^{-1}	$\mu_\delta \pm \sigma$ mas yr^{-1}	COR mas	$N_*, N_o, \Delta T$ yr
1341-3052	205.2984590, − 30.8811496	2011.21	26.64 ± 4.08	19.13 ± 0.77	− 159.89 ± 0.60	0.43	28, 28, 8.01
1404-3159	211.2071517, − 31.9925574	2009.57	45.03 ± 2.48	335.66 ± 0.60	− 19.96 ± 1.01	0.43	47, 28, 8.01
1425-3650	216.3656475, − 36.8411210	2014.21	79.64 ± 3.60	− 278.39 ± 0.75	− 466.42 ± 1.16	0.41	34, 25, 8.89
1438-1309	219.7296481, − 13.1530385	2011.22	30.65 ± 3.06	147.37 ± 0.79	− 42.26 ± 0.88	0.21	28, 31, 8.89
1441-0945	220.4042039, − 9.7664631	2008.65	25.83 ± 2.74	− 193.91 ± 0.77	− 12.71 ± 0.50	0.43	16, 28, 8.90
1457-2121	224.3159237, − 21.3687893	2014.21	162.09 ± 9.54	1034.15 ± 2.71	− 1694.83 ± 2.51	0.31	30, 30, 8.89
1507-1627	226.9482001, − 16.4636115	2011.23	135.86 ± 1.59	− 145.81 ± 0.37	− 890.96 ± 0.50	0.35	31, 29, 8.90
1520-4422B	230.0065948, − 44.3786651	2008.26	48.50 ± 3.09	− 625.08 ± 0.64	− 390.15 ± 1.20	0.35	210, 33, 8.90
1523-2347	230.7768454, − 23.7980225	2007.27	29.06 ± 1.58	− 157.48 ± 0.39	− 15.95 ± 0.57	0.32	20, 28, 8.90
1530-8145	232.6076191, − 81.7608821	2014.21	8.34 ± 2.22	− 578.30 ± 0.48	− 278.02 ± 1.33	0.50	43, 24, 8.01
1534-2952	233.7078856, − 29.8751170	2008.26	60.27 ± 3.11	98.39 ± 0.63	− 258.96 ± 0.82	0.39	82, 28, 8.90
1539-0520	234.9263159, − 5.3449277	2009.56	60.03 ± 2.22	599.36 ± 0.79	107.77 ± 0.54	0.47	17, 38, 8.02
1547-2423	236.9461995, − 24.3974581	2008.16	25.51 ± 1.80	− 139.11 ± 0.60	− 129.20 ± 0.54	0.40	34, 37, 8.90
1548-1636	237.2423980, − 16.6009345	2011.23	35.58 ± 2.10	− 199.25 ± 0.59	− 116.78 ± 0.70	0.41	15, 31, 8.90
1618-1321	244.6873677, − 13.3586183	2014.22	22.59 ± 1.87	− 105.68 ± 0.54	− 79.15 ± 0.74	0.35	22, 33, 8.90
1620-0416	245.1078344, − 4.2755193	2014.21	35.58 ± 12.97	− 415.26 ± 1.17	− 11.38 ± 1.02	0.28	30, 16, 8.90
1633-0640	248.4964332, − 6.6826880	2011.22	35.67 ± 4.08	− 274.45 ± 1.61	− 230.01 ± 1.61	0.28	60, 24, 8.89
1636-0034	249.0022053, − 0.5819366	2009.24	25.84 ± 2.81	− 360.80 ± 1.73	− 209.72 ± 1.82	0.35	28, 22, 3.95
1645-1319	251.3409440, − 13.3332700	2009.38	88.28 ± 1.30	− 357.22 ± 0.60	− 800.00 ± 1.14	0.33	51, 31, 8.90
1705-0516	256.4518081, − 5.2797930	2011.22	53.30 ± 1.26	120.84 ± 0.55	− 115.79 ± 0.44	0.33	24, 37, 6.94
1707-0558	256.8478553, − 5.9736454	2010.63	89.26 ± 2.20	91.55 ± 0.76	18.69 ± 0.60	0.33	72, 31, 8.90
1750-0016	267.6022252, − 0.2702677	2014.21	110.43 ± 1.08	− 399.46 ± 0.55	202.81 ± 0.69	0.30	62, 38, 6.94
1753-6559	268.4379566, − 65.9997520	2008.26	65.74 ± 2.67	− 50.27 ± 1.51	− 334.23 ± 1.13	0.47	64, 47, 6.94
1828-4849	277.1497034, − 48.8177596	2009.72	78.44 ± 4.87	229.11 ± 1.71	86.09 ± 2.50	0.36	104, 23, 8.48
1840-5631	280.0788728, − 56.5210301	2007.27	11.02 ± 4.66	− 84.46 ± 2.65	− 166.76 ± 7.15	0.40	58, 27, 4.28
1928-4356	292.2163563, − 43.9409577	2010.60	35.06 ± 4.63	66.34 ± 1.52	− 284.68 ± 2.71	0.29	44, 34, 8.10
1936-5502	294.0088562, − 55.0430750	2009.33	46.82 ± 2.05	202.39 ± 1.25	− 287.87 ± 2.37	0.31	30, 38, 3.89
1956-1754	299.0643263, − 17.9070956	2009.73	25.82 ± 1.58	6.18 ± 0.65	− 27.52 ± 0.79	0.38	42, 38, 8.10
2002-0521	300.7107882, − 5.3650469	2010.59	59.76 ± 7.30	− 120.39 ± 2.63	− 107.71 ± 3.42	0.46	72, 32, 8.10
2011-6201	302.9870707, − 62.0212510	2009.72	11.45 ± 3.98	314.94 ± 2.23	− 394.10 ± 2.25	0.34	33, 26, 3.88
2023-5946	305.8693574, − 59.7811637	2011.55	10.89 ± 5.01	70.67 ± 3.36	− 14.38 ± 1.77	0.39	23, 25, 3.88
2026-2943	306.5661130, − 29.7212734	2015.76	35.29 ± 7.00	17.84 ± 2.10	− 355.40 ± 2.43	0.23	15, 27, 8.10
2041-3506	310.4286404, − 35.1127254	2010.63	22.91 ± 3.45	40.39 ± 1.13	− 134.48 ± 1.42	0.34	28, 24, 8.09
2045-6332	311.2604376, − 63.5357349	2008.65	50.55 ± 2.80	75.33 ± 1.10	− 204.59 ± 0.99	0.46	17, 28, 8.10
2057-0252	314.4753838, − 2.8753406	2010.33	70.40 ± 2.70	3.13 ± 0.89	− 90.84 ± 0.89	0.52	14, 31, 8.10
2101-2944	315.4683482, − 29.7347644	2008.64	30.78 ± 5.81	65.71 ± 4.32	3.09 ± 17.68	0.26	12, 5, 1.95
2104-1037	316.0640199, − 10.6278714	2010.59	55.89 ± 4.42	596.79 ± 2.40	− 284.53 ± 2.69	0.34	10, 7, 2.92
2107-4544	316.9757837, − 45.7351717	2009.73	34.88 ± 7.03	91.34 ± 2.80	− 15.52 ± 2.63	0.46	12, 26, 8.10
2130-0845	322.6869987, − 8.7558442	2009.38	36.98 ± 9.48	350.92 ± 2.38	− 30.69 ± 1.19	0.47	11, 23, 8.10
2132-1452	323.2037671, − 14.8823207	2009.73	31.53 ± 12.63	− 100.62 ± 5.43	− 145.93 ± 7.32	0.30	24, 23, 3.88
2150-7520	327.5755503, − 75.3442968	2010.46	42.67 ± 8.28	881.96 ± 2.16	− 297.71 ± 1.92	0.42	12, 22, 8.10
2157-5534	329.4546555, − 55.5783892	2010.46	35.12 ± 3.85	43.92 ± 0.98	− 10.75 ± 1.06	0.36	9, 27, 8.10
2158-1550	329.5190934, − 15.8362139	2009.38	44.69 ± 7.32	39.20 ± 2.07	− 57.36 ± 3.23	0.24	17, 13, 3.88
2204-5646	331.0642768, − 56.7897998	2007.67	277.37 ± 14.60	4004.97 ± 9.65	− 2575.05 ± 9.02	0.39	18, 13, 3.88
2206-4217	331.6879882, − 42.2897395	2009.56	36.79 ± 14.87	126.88 ± 15.20	− 176.59 ± 8.13	0.37	13, 12, 2.93
2209-2711	332.3409290, − 27.1928581	2015.76	54.13 ± 9.20	− 5.95 ± 2.36	− 122.17 ± 2.72	0.26	17, 19, 8.09
2213-2136	333.4372519, − 21.6024355	2007.67	41.68 ± 12.46	2.23 ± 9.87	− 52.05 ± 5.21	0.30	11, 6, 1.89
2224-0158	336.1840312, − 1.9838795	2007.67	83.69 ± 4.06	471.41 ± 0.85	− 863.28 ± 1.92	0.56	11, 13, 8.10
2252-1730	343.0459795, − 17.5033484	2009.96	50.09 ± 4.62	397.32 ± 0.91	136.27 ± 1.11	0.31	9, 24, 8.01
2254-2840	343.7164432, − 28.6736748	2009.38	32.87 ± 3.60	− 3.48 ± 2.80	31.90 ± 2.27	0.21	14, 8, 2.06
2255-0034	343.8710403, − 0.5765119	2011.55	20.20 ± 6.28	− 41.42 ± 1.49	− 176.89 ± 1.86	0.28	9, 28, 8.09
2310-1759	347.5770339, − 17.9868960	2009.73	24.75 ± 4.79	32.85 ± 1.19	− 285.87 ± 1.08	0.35	8, 9, 8.11
2318-1301	349.7267431, − 13.0204057	2007.67	81.47 ± 13.99	− 797.18 ± 4.81	− 255.13 ± 6.07	0.20	10, 14, 6.03
2330-0347	352.5948267, − 3.7885807	2009.96	42.38 ± 9.51	203.44 ± 1.92	12.48 ± 1.21	0.19	8, 20, 8.11
2346-5928	356.6121968, − 59.4783859	2010.86	15.44 ± 3.28	251.08 ± 0.97	56.34 ± 0.83	0.50	11, 30, 8.10
2351-2537	357.9614199, − 25.6263449	2009.73	41.21 ± 4.45	341.29 ± 1.10	198.30 ± 1.16	0.36	7, 17, 8.10

(COR), number of observations used in the final solution (N_*), number of anonymous objects used as references in the transformation of sequence frames to the base frame (N_o), epoch coverage of the frames in the final solution (ΔT). The parallax errors range from 1.0 to 15.5 mas with a median of 3.8 mas. We also constructed a comparison sample of objects from the literature with parallaxes mainly from the list maintained by Trent Dupuy[1] (Dupuy & Liu 2012; Dupuy & Kraus 2013; Liu, Dupuy & Allers 2016) adding 238 L0 to T8 objects.

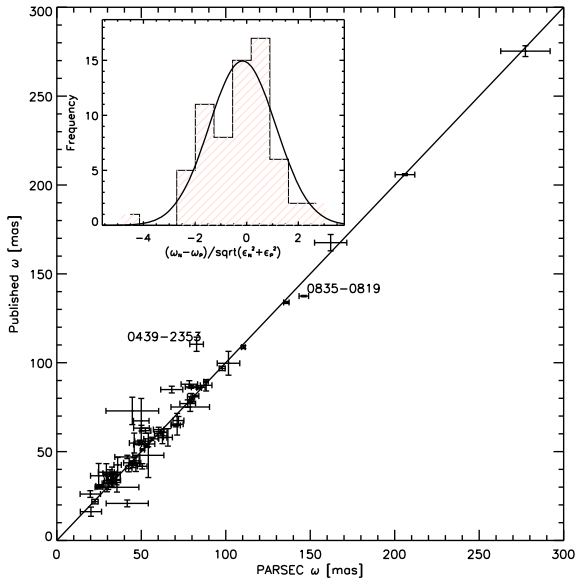[1] www.as.utexas.edu/~tdupuy/plx/

Figure 2. Published versus PARSEC parallaxes. The solid line is the locus expected if the published and new values are equal. The two labelled objects have published and PARSEC parallaxes that differ by more than three times their combined errors and are discussed in Section 3.1. The insert shows the distribution of the quantity $\frac{\varpi_N - \varpi_P}{\sqrt{\sigma_N^2 + \sigma_P^2}}$ as discussed in Section 3.1.

3.1 Comparison to published parallaxes

There are published estimates of the parallaxes for 66 PARSEC targets of which 24 were preliminary values from this program. The preliminary values were found using different reduction procedures and different epoch spans, hence we consider them as independent estimates. In Fig. 2, we plot the 66 published values listed in Table 1 versus results presented here from Table 2.

Only two objects, 0439-2353 and 0835-0819, have parallaxes that differ by more than three times the combined errors so warrant further consideration. For 0439-2353, Faherty et al. (2012) find 110.4 ± 4.0 mas while we obtain 79.75 ± 3.36 mas. The Faherty et al. observational coverage was 3 yr with 14 nights while we have 8 yr and 18 nights. We estimated the photometric parallax to be ∼80 mas using the Vrba et al. (2004) absolute magnitude calibrations which is closer to the PARSEC estimate. The difference between the Faherty et al. parallax and the photometric parallax could be explained if the object is an unresolved binary but the residuals show no non-linear motion and a spectroscopic investigation for binarity by Manjavacas et al. (2016) also found no evidence. We therefore consider our value more probable. For 0835-0819, we obtain 146.19 ± 2.82 from 35 observations over 8.9 yr while Weinberger et al. (2016) find 137.5 ± 0.4 using observations in 17 epochs over 6.2 yr. The difference is just over three times the combined error and the quoted error from Weinberger et al. (2016) is very low considering the observations were made on a similar system so we believe that the larger than 3σ difference is probably because the errors are underestimated.

For the 66 PARSEC dwarfs with published parallaxes, we calculated the quantity $\frac{\varpi_N - \varpi_P}{\sqrt{\sigma_N^2 + \sigma_P^2}}$, where ϖ is the parallax, σ the quoted errors and the subscripts N and P represent the new and published values, respectively. If the measures are unbiased and the errors are precise we expect this quantity to follow a Gaussian distribution with a mean of zero and a standard deviation of one. For the 66 common objects, the mean is -0.1 and the standard deviation is

Table 3. Wide binary systems in the PARSEC program.

Target companion	$\varpi \pm \sigma$ (mas)	$\mu_\alpha \pm \sigma$ (mas yr^{-1})	$\mu_\delta \pm \sigma$ (mas yr^{-1})
0004-4044[1,a]	77.5 ± 4.6	668.7 ± 1.3	-1498.2 ± 1.3
GJ 1001A	86.4 ± 4.5	672.3 ± 1.2	-1500.1 ± 1.4
0235-2331	41.7 ± 7.4	95.0 ± 4.8	38.9 ± 10.5
GJ 1048A[2,b]	45.7 ± 5.8	92.8 ± 3.5	-18.1 ± 36.0
1004-3335[c]	45.8 ± 2.9	343.6 ± 0.6	-345.4 ± 0.7
LHS 5166	49.8 ± 2.2	349.6 ± 0.4	-348.8 ± 0.5
1441-0945[d]	25.8 ± 2.7	-193.9 ± 0.8	-12.7 ± 0.5
G 124-6	23.7 ± 3.2	-203.5 ± 0.8	-4.4 ± 1.8

Note. Objects with published parallaxes 1: 76.9 ± 4.0 (Henry et al. 2006), 2: 47.2 ± 0.3 (Gaia Collaboration et al. 2016b).
Reference for binarity. *a*: Golimowski et al. (2004), *b*: Wilson et al. (2001), *c*: Seifahrt et al. (2005a), and *d*: Seifahrt et al. (2005b).

1.3. Applying the t-test at the 95 per cent level we find the mean is not significantly different from zero, e.g. $P(t) = 0.06$, while applying the F-test we find the σ is significantly different from one, e.g. $P(F) = 0.0001$. Since the σ is greater than one the implication is that the errors are underestimated. The median PARSEC error is larger than the median published error even though the programs were often very similar, however, without a standard comparison it is difficult to isolate. The *Gaia* sample should allow a complete characterization of the errors of different procedures which can then be applied to objects that are fainter than the *Gaia* limit in those programs.

3.2 Comparisons within binaries

Binary systems are a good test for parallax determinations and in particular for the quality assurance of errors. Components in binary systems can be considered to be at the same distance and if the system is a wide binary it is appropriate to make independent solutions. In the PARSEC sample, there are four companions observable (e.g. in the field of view and not so bright that they saturate) and in Table 3 we reproduce the parallaxes and proper motions of the PARSEC targets and the companions determined in this program. No parallaxes or proper motions differ by more than 2σ between the PARSEC values or the published values but this sample is too small to test the precision of the error estimates.

4 PHOTOMETRIC CONSIDERATIONS

4.1 Internal photometry

During every observation, we obtain precise relative photometry. The highest observation frequency for our objects was monthly so the sampling is not sufficient to find short-period photometric variations but we can look for long-term variations. For each object, we transformed the magnitudes to the instrumental magnitude system of the base frame using the anonymous reference stars with iterative 3σ clipping and then found the linear correlation between instrumental magnitudes and observation time of the target. The slopes for most targets were within 3σ of zero but two objects, 0614-2019 and 1122-3916, were found to have significant slopes of 0.0079 ± 0.0021 and 0.0124 ± 0.0037 mag yr^{-1}, respectively. For both objects, the χ^2 sum of the two parameter fit was a statistically significant improvement over a one-parameter fit. In Fig. 3, we reproduce the magnitude variation of these two objects over the observational sequence. Possible explanations for a long-term
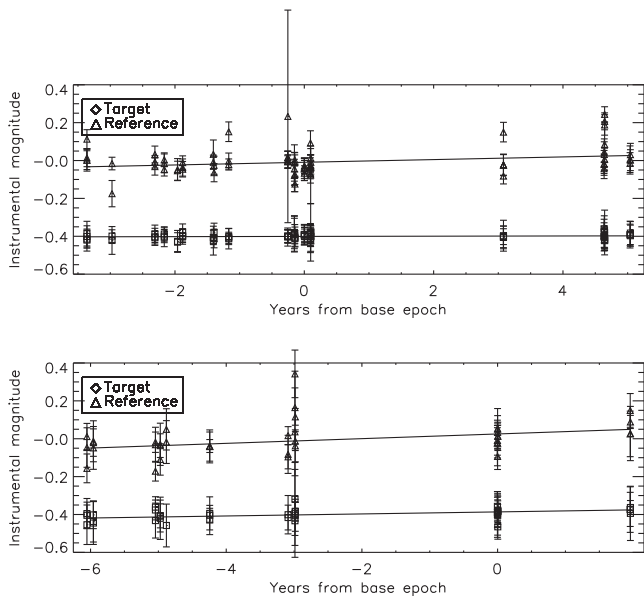
Figure 3. Instrumental *z*-magnitude variations as a function of time for 0614-2019 (upper plot) and 1122-3916 (lower plot). As a comparison in each plot, we have included an anonymous object that is nearby in position and magnitude space and included its variation offset by 0.4 mag.

photometric variation are discussed in Smart et al. (2017a) for Y dwarfs and in the K2 Ultracool Dwarfs Survey (and references therein Paudel et al. 2018) or the Weather on Other Worlds program (and references therein Miles-Páez et al. 2017) for L/T dwarfs.

4.2 Literature photometry

We compiled photometry on standard systems for the Full Sample from the large optical and infrared surveys: 2MASS (Skrutskie et al. 2006); *Gaia* (Gaia Collaboration et al. 2016a); Pan-STARRS (Chambers et al. 2016); Sloan Digital Sky Survey (SDSS; Ahn et al. 2014); Visible and Infrared Survey Telescope for Astronomy (VISTA) VISTA Variables in the Via Lactea (VVV; Minniti et al. 2010) – VISTA Magellanic Survey (VMC; Cioni et al. 2011) – VISTA Hemisphere Survey (VHS; McMahon et al. 2013) surveys; UKIRT Infrared Deep Sky Survey (UKIDSS; Lawrence et al. 2007); and *WISE* (Ahn et al. 2014). Using these surveys, it was possible to obtain homogeneous magnitudes in bands ranging from Gunn G to *WISE* W3 (the Gunn U and *WISE* W4 bands were not included as the number of objects with reliable magnitudes was very low). The number of independent magnitude measures ranged from 3 to 16 with a mean of 10 per target.

For those objects with published parallaxes, we took the weighted mean of the PARSEC and published value with no outlier rejection. The complete dataset of 356 objects with photometry and parallaxes is available online here.

4.3 Absolute magnitudes

In Fig. 4, we plot the absolute magnitudes of the PARSEC sample in the 2MASS *J* and *WISE* W2 bands versus near-infrared spectral types. The crosses represent the PARSEC objects with propagated errors in the magnitude axis and an assumed error of 0.5 types in the spectral type axis. The grey area represents the 1σ confidence limits of a second-order fit to objects with published parallaxes. A fit to just the PARSEC sample is within 1σ of fits to the Full Sample in all
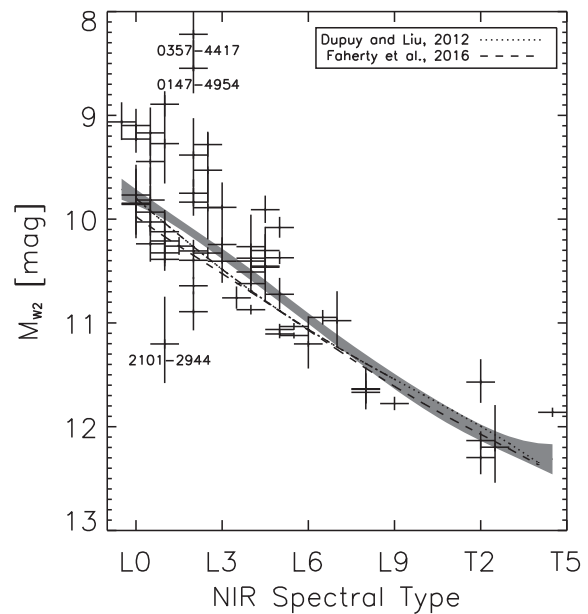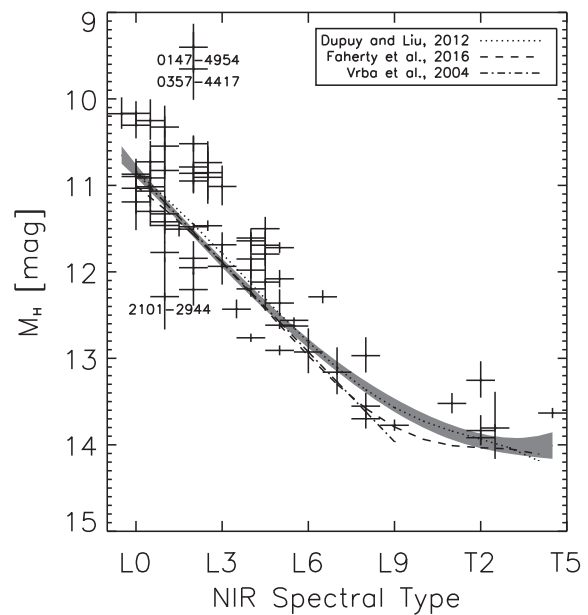
Figure 4. PARSEC absolute magnitudes in the 2MASS *H* (top) and *WISE*W2 (bottom) bands versus near-infrared spectral types. The length of the symbol arms represent the error which for spectral types is assumed to be 0.5 types. The grey area represents 1σ confidence limits for a fit to published objects using literature parallaxes. We have included as comparisons the polynomial relations from (Dupuy & Liu 2012), Faherty et al. (2016), and for *H* only (Vrba et al. 2004) as indicated in the legend.

magnitude bands. As a comparison, we have plotted the polynomial relations derived in the studies of Dupuy & Liu (2012), Faherty et al. (2016), and for *H* only (Vrba et al. 2004).

In Table 4, we report the polynomial fits of the absolute magnitudes to the published spectral types of the form:

$$AbsMag = P1 + P2 * Spt + P3 * Spt^2, \quad (1)$$

where AbsMag is the absolute magnitude in the passband indicated in column 1 of Table 4; $P1...P3$ are the parameters in columns 3–5

Table 4. Absolute magnitude calibrations using Full Sample.

Passband	N	P1	P2	P3	σ
r	73	−1.604e+02 ± 8.648e+01	4.558e+00 ± 2.375e+00	−2.867e−02 ± 1.630e−02	0.735
i	109	−4.109e+01 ± 2.947e+01	1.071e+00 ± 7.969e−01	−3.661e−03 ± 5.382e−03	0.521
z	100	−1.435e+02 ± 2.123e+01	3.903e+00 ± 5.698e−01	−2.351e−02 ± 3.819e−03	0.453
y	106	−1.638e+02 ± 2.111e+01	4.446e+00 ± 5.664e−01	−2.733e−02 ± 3.796e−03	0.492
Y MKO	27	−1.710e+02 ± 3.006e+01	4.658e+00 ± 7.970e−01	−2.906e−02 ± 5.271e−03	0.400
J	170	−1.530e+02 ± 1.372e+01	4.129e+00 ± 3.600e−01	−2.543e−02 ± 2.354e−03	0.558
H	167	−8.511e+01 ± 1.136e+01	2.317e+00 ± 2.983e−01	−1.353e−02 ± 1.953e−03	0.456
K_s	160	−4.320e+01 ± 1.224e+01	1.181e+00 ± 3.223e−01	−5.964e−03 ± 2.117e−03	0.427
J MKO	132	−1.603e+02 ± 1.730e+01	4.335e+00 ± 4.539e−01	−2.688e−02 ± 2.969e−03	0.895
H MKO	40	−1.116e+02 ± 2.216e+01	3.017e+00 ± 5.759e−01	−1.811e−02 ± 3.730e−03	0.438
K MKO	84	−4.578e+01 ± 1.474e+01	1.258e+00 ± 3.871e−01	−6.523e−03 ± 2.534e−03	0.596
W1	162	2.264e+01 ± 1.035e+01	−5.415e−01 ± 2.716e−01	5.167e−03 ± 1.777e−03	0.415
W2	159	−1.634e+01 ± 1.118e+01	5.291e−01 ± 2.932e−01	−2.236e−03 ± 1.917e−03	0.430
W3	114	−4.693e+01 ± 1.778e+01	1.394e+00 ± 4.694e−01	−8.431e−03 ± 3.089e−03	0.507

Note. Coefficients of polynomial fits to absolute magnitudes derived using parallaxes from Full Sample and large all sky photometry as described in Section 4.3.

of Table 4 and *SpT* is the spectral type in numerical format, e.g. L0 = 70, L1 = 71 ... T5 = 85. The absolute magnitude in the passbands *r* to *y* refer to optical spectral types, the passbands *J* to *W3* refer to NIR spectral types. For each passband, we removed any objects which were tagged as unresolved binaries or which had a $\varpi/\sigma < 5$ and fitting was carried out using iterative outlier rejection of objects with residuals larger than three times the overall fit error.

The labelled objects in Fig. 4, 0147-4954, 0357-4417, and 2101-2944, are more than 3σ from the mean absolute magnitude versus spectral type locus in at least two passbands. 0147-4954 was included as a L2 but was reclassified as a M9 in Marocco et al. (2013), at this spectral type it is not over luminous. 0357-4417 is a known unresolved binary (Bouy et al. 2003) hence the brighter than average observed absolute magnitude. 2101-2944 is underluminous at the 3σ level in the *W1* and 2MASS *K* bands but shows no underluminosity in other bands and its spectra does not show any sign of peculiarity (Marocco et al. 2013) so the underluminosity in these two bands is unexplained.

4.4 Spectral energy distribution analysis

Using the multiband photometry and our distances, we are able to generate spectral energy distributions (SEDs) for the PARSEC objects. While the SEDs contain less information than the spectra, the instrumental differences in spectral observations render the SEDs globally more homogeneous. To compare these to models, we made use of the VO SED Analyzer (VOSA; Bayo et al. 2008) which provides χ^2 and Bayesian fitting to an array of models and templates. For this data, we adopted the χ^2 fitting to BT-Settl models (Allard, Homeier & Freytag 2012) with the following limits: $700 < T_{eff} < 4000$ K, $3.5 < \log g < 5.5$ and $-1 < \frac{Fe}{H} < 0.5$. We also limited the absorption in the *V* band to 0.001 and turned off the excess fitting option as the non-black body distribution of the spectra of these objects was causing the excess fitting procedures to ignore the mid-IR magnitudes.

As an example in Fig. 5, we plot the VOSA fit of 0227-1624 to the BT-Settl model spectra. 0227-1624 is a 16th *z*-band magnitude L1/L0.5 object at 20 pc with a 8 per cent error on the distance for which we have magnitudes in 11 bands. The model slightly underestimates the near- and mid-infrared bands but follows well for the optical bands. Reasons for this over luminosity are beyond the scope of this paper as it will require a more in-depth study of the models and the fitting of VOSA.

The *Gaia G* observation is plotted in orange because we manually removed it from the fit. We find the nominal *G* passband tends to over estimate the flux of the L and T dwarfs which can be seen in Fig. 5. This systematic excess is also reflected in the model (the blue points) as this uses the *G* passband for the transformation, however, we felt this known systematic error made using the *Gaia* magnitude for the 38 objects in the *Gaia* DR1 to constrain the fits premature. The problem of the *G* passband is noted in the *Gaia* documentation,[2] and there is an empirical correction proposed(Maíz Apellániz 2017).

In Fig. 6, we plot the RAD1 radius from the VOSA fits to BT-Settl models against the near-infrared spectral types. RAD1 is the 'scaling radius', i.e. the radius required to fit the observations to the model based on the parallactic distance. From the PARSEC sample, we removed all objects which are known or suspect unresolved binary systems and known or candidate moving group objects (see Section 5.3) leaving 60 objects. We removed the moving group objects as these are in general young and we wanted to be sure that our sample was dominated by objects older than 1 Gyr. In Fig. 6, the targets plotted as diamonds are literature objects and the PARSEC sample are plotted as asterisks. The radius of objects with ages greater than 1 Gyr in this spectral range is predicted to be a minimum at the spectral type that corresponds to the hydrogen burning limit (e.g. Chabrier et al. 2009; Burrows, Heng & Nampaisarn 2011). Objects with earlier spectral types than this limit are in hydrostatic equilibrium and the radius decreases with the spectral type. Objects with later spectral types than this limit are degenerate and in this case the radius increases with the spectral type. Hence, we expect to find a minimum RAD1 that corresponds to the spectral type of objects at the hydrogen burning limit.

We experimented with a grid of trial spectral types fitting the RAD1 to the spectral type on either side of the trial value with simple straight line fits. In each fit, we weight a common point given by the median around the trial value to guide continuity. As an example in Fig. 6, we have plotted the two line fit of the observations assuming a minimum at L6. We then calculate the minimum χ^2 of the combined fits, which formally occurs if we choose the trial value between spectral types L3 and L4, however there is no significant difference between L2 and L6, the minimum is not well defined. In Dieterich et al. (2014), for a smaller more refined sample they find the position of the minimum at L2.5, which
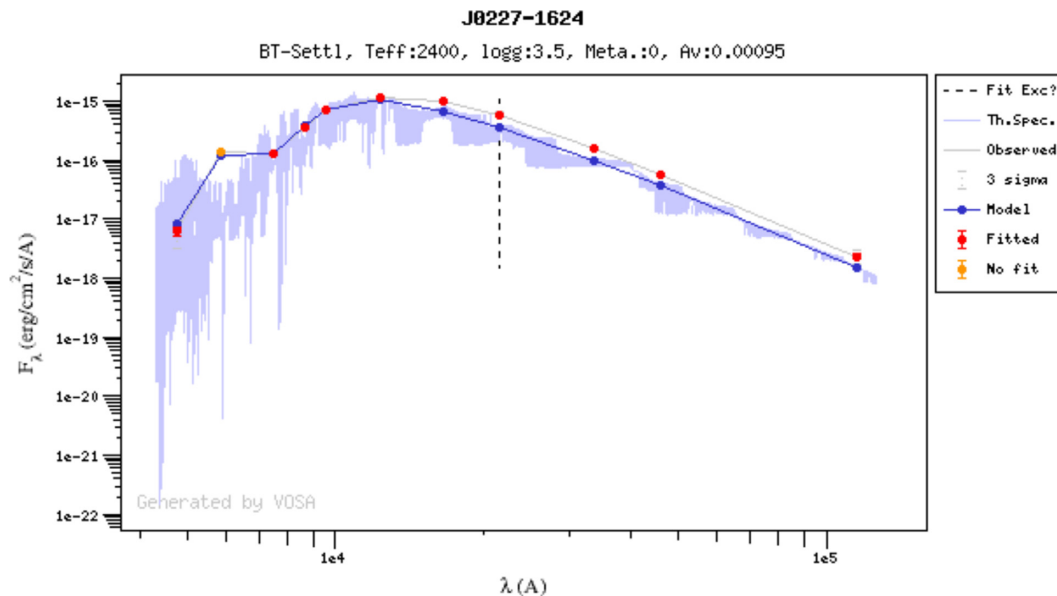
[2] gaia.esac.esa.int/documentation/

Figure 5. An example VOSA χ^2 fitting of the 0227-1624 spectral energy distribution to BT-Settl models. The optical to *J* bands appear to fit well but the model underestimates the flux in the other near and mid-infrared bands reasons for which are discussed in Section 4.4.
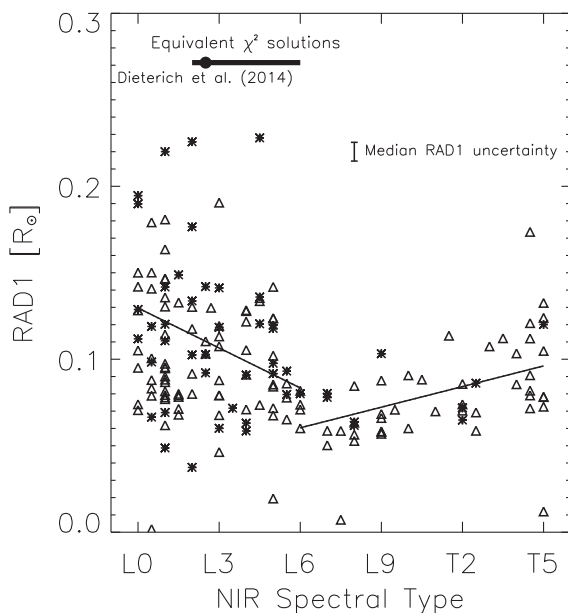

Figure 6. Scaling radius (RAD1) in solar radii from VOSA BT-Settl model fitting versus near-infrared spectral types. The asterisks represent the 60 PARSEC objects and the diamonds represent the 132 literature objects that are not suspect binary or moving group members. The error bar in the top of the graph is the median error from VOSA for RAD1. The two lines represent two simple straight fits of RAD1 to spectral type on either side of L6. The black bar represents the range of solutions where the χ^2 minimum did not vary significantly while the black circle is the minimum radius found by Dieterich et al. (2014). The sample and fitting procedure are discussed in Section 4.4.

is the early end of our window. In Dieterich et al. (2014), they use tailor made SED fitting that is calibrated with radii of objects with radii measurements from interferometric observations so we expect this to be a more robust estimate.

The larger sample we have included here is going to cover a range of ages, metallicities, and masses and as discussed in Burrows

et al. (2011) the position of the minimum is dependent on age and metallicity so as this is a mixed population we do not expect to have a unique clear minimum. In addition, even for a given age the minimum may not be a single distinct value, for example in the case of halo UCDs there is a narrow mass range in which unsteady nuclear fusion occurs (Zhang et al. 2017). If this occurs even over a smaller range for younger UCDs it would result in spreading out of the minimum. The general trend is of a steep dependence in the hydrogen burning regime and a flatter change in the degenerate regime predicted by Burrows et al. (2011) is however confirmed.

5 KINEMATIC CONSIDERATIONS

5.1 Solar motion and velocity ellipsoids

To calculate the *UVW* velocity components in the galactic reference frame in addition to position, proper motion, and parallax, we also require radial velocities. We follow the general procedure of Johnson & Soderblom (1987) except we use the transformation matrix from equatorial coordinate to galactic coordinates taken from the introduction to the HIPPARCOS catalogue (ESA 1997). For the PARSEC sample 20 objects have published radial velocities and for the Full Sample 38 objects. For the objects without radial velocities, we estimate only the two components least impacted by assuming a zero radial velocity following the recipe in Lépine et al. (2013). From the Full Sample of PARSEC and published L0–T8 dwarfs of 356 objects, we obtained 284, 306, 180 *U*, *V*, *W* components, respectively.

To isolate those dwarfs that are part of the thin disk population, we use 3σ clipping in each element and remove 34 objects from the Full Sample of 356 which includes 16 from the PARSEC subset. This is a simple efficient method for the removal of non-thin disk and outlier objects. In Table 5, we report the mean and standard deviations of the velocity components for the PARSEC, published and Full Sample after this cleaning.

The velocities are all heliocentric so the mean velocity vector indicates the anti-motion of the Sun relative to this sample. From

Table 5. Mean and dispersions of *UVW* velocity components. ν is the generic symbol used to indicate the components *U*, *V*, or *W*.

Direction and sample	$\bar{v} \pm \sigma_{\bar{v}}$ km s^{-1}	σ_ν km s^{-1}	N_σ	$\sigma_{|W|\nu}$ km s^{-1}	$N_{\sigma_{|W|\nu}}$
U PARSEC	-5.3 ± 2.5	22.6	85	22.5	29
Not PARSEC	-5.5 ± 1.8	25.1	200	27.4	73
Full	-5.4 ± 1.4	24.4	285	26.1	102
V PARSEC	-12.8 ± 1.7	15.6	88	22.4	32
Not PARSEC	-12.5 ± 1.0	15.2	220	19.9	93
Full	-12.6 ± 0.9	15.3	308	20.6	125
W PARSEC	-7.4 ± 2.1	14.4	46	12.4	46
Not PARSEC	-7.7 ± 1.2	14.2	133	12.1	133
All	-7.6 ± 1.1	14.2	179	12.2	179

Table 5, we would estimate the Solar motion compared to the Full Sample to be $(U, V, W)_\odot = (5.4 \pm 1.4, 12.6 \pm 0.9, 7.6 \pm 1.1)$ km s^{-1}, which can be compared directly to the Sun's velocity components inferred by larger stellar groups, e.g. Schönrich, Binney & Dehnen (2010): $(U, V, W)_\odot = (11.10^{+0.69}_{-0.75}, 12.24^{+0.47}_{-0.47}, 7.25^{+0.37}_{-0.36})$ km s^{-1}, and Francis & Anderson (2009): $(U, V, W)_\odot = (7.5 \pm 0.1, 13.5 \pm 0.3, 6.8 \pm 0.1)$ km s^{-1}. Considering the large uncertainties, and given the agreement in the direction of rotation (*V*) indicate that our sample, as a whole, is not moving very differently from the local standard of rest.

The dispersions of the velocities (σ_o) are the result of the dynamical evolution of our sample in the galactic disk. The dispersions derived here, $(\sigma_U, \sigma_V, \sigma_W) = (24.4, 15.3, 14.2)$ km s^{-1}, are consistent but generally smaller than other studies of L and T dwarfs, e.g. Zapatero Osorio et al. (2007): $(30.2, 16.5, 15.8)$ km s^{-1}, Faherty et al. (2009): $(22, 28, 17)$ km s^{-1}, and Seifahrt et al. (2010): $(33.8, 28.0, 16.3)$ km s^{-1}. The lower values may be because of our stringent 3σ clipping or the fact that our sample are objects with parallaxes, which for a given spectral type are in general brighter, and hence often younger.

5.2 Age estimation

Wielen (1977) finds that dynamical heating provides a relation between observed velocity dispersion and mean age of a given stellar population. Rearranging the velocity-dependent diffusion equation (13) from Wielen for ages less than 3 Gyr, we get:

$$\tau = \frac{\tilde{\sigma}^3_{|W|\nu}(\tau) - \sigma^3_0}{1.5\gamma_\nu}, \tag{2}$$

where τ is the mean age, $\sigma_0 = 10$ km s^{-1} and $\gamma_\nu = 1.4 \times 10^{-5}$ (km/s)^3 yr^{-1} and $\tilde{\sigma}_{|W|\nu}$ is total of the $|W|$ weighted velocity components, $\sigma_{|W|\nu}$ column in Table 5. These are calculated using:

$$\sigma^2_{|W|U} = \sum |W|U^2 / \sum |W|$$
$$\sigma^2_{|W|V} = \sum |W|V^2 / \sum |W|$$
$$\sigma^2_{|W|W} = 0.5 * \sum |W|W^2 / \sum |W|$$

from Wielen (1977). The sum of the $|W|$ weighted velocities are 35.4 km s^{-1} for the PARSEC sub-sample and 34.1 km s^{-1} for all objects corresponding, respectively, to an age of 2.1 and 1.8 Gyr. Using equation (16) from Wielen for ages >3 Gyr, we also get an age of less than 3 Gyr, so equation (13) is more appropriate.

These estimates of the age are younger than the $\sim$5.1 Gyr in Seifahrt et al. (2010) and the 3.4$\sim$3.8 Gyr from Burgasser et al.

(2015) with similar samples and procedures, though both studies benefitted from having radial velocities for all their target which we do not have. Our estimates are however in agreement with $\tau = 1.7 \pm 0.3$ Gyr found in Wang et al. (2018) using a similar sample/procedure and also in Dupuy & Liu (2017), where the median age is 1.3 Gyr for L dwarfs from dynamical masses and luminosities combined with evolutionary models. The reason for this younger value may be, as before, a result of our sample cleaning or because we are dominated by brighter examples. The *Gaia* results should be complete to some limiting magnitude so it will be interesting to see what they reveal – especially since the full *Gaia* dataset will significantly constrain kinematically based ages.

5.3 Moving group membership

We used the packages LocAting Constituent mEmbers In Nearby Groups[3] (hereafter LACEwING; Riedel et al. 2017) and Bayesian Analysis for Nearby Young AssociatioNs Σ[4] (hereafter BANYAN Σ; Malo et al. 2013; Gagné et al. 2014; Gagné et al. 2018) to assess membership of our sample to known moving groups starting from the assumption that they are all field objects – e.g. that we have no spectral or colour evidence of youth. This assumption is a conservative starting point as some objects are known to have signs of youth and are often known moving group candidates as indicated by *MG* in column 6 of Table 1. Since we start from a conservative position our moving group candidate indication should be more robust and homogeneous.

The calculation of probability is different between LACEwING and BANYAN Σ, in the first case the probabilities are considered independent while in the second case the probabilities are required to sum up to 100 per cent, i.e. the object is either in one of the included moving groups or it is a field object. This generally leads to LACEwING having lower probabilities. Based on a comparison of the objects that overlap we select as candidate moving group members those with 80 per cent probability for BANYAN Σ and 50 per cent for LACEwING.

We find 20 objects from BANYAN Σ and 21 from LACEwING. The candidates that are not already published in the literature are listed in Table 6 along with the name of the moving group and the probability of membership. Most of these candidates do not have radial velocities, when these become available these probabilities should be revisited. Of the 13 PARSEC objects indicated in the literature as moving group members, 6 were not confirmed by either procedure: 0357-4417 (Gagné et al. 2014), 1058-1548 (Gagné et al. 2015b), 1154-3400 (Gagné et al. 2015a), 1547-2423 (Gagné et al. 2015a), 1707-0558 (McElwain & Burgasser 2006), 2045-6332 (Gálvez-Ortiz et al. 2010). For three of these, 0357-4417, 1154-3400, and 1707-0558, the previous indication was made without a parallax which provides a strong new constraint.

6 CONCLUSIONS

We have presented parallaxes and proper motions for 118 objects. Using this new sample, we have examined their photometric and kinematic properties. In the PARSEC sample, we have identified candidate moving group members, found objects with long term photometric variations, estimated the age of a local sample of L and T dwarfs and confirmed global trends of the predicted radius versus

---

[3]github.com/ariedel/lacewing
[4]github.com/jgagneastro/banyan_sigma_idl

Table 6. New moving group candidates with LACEwING selecting only probabilities greater than 50% and BANYAN Σ selecting only non-field objects and probabilities greater than 80%.

PARSEC Target	BANYAN Σ Group, prob.	LACEwING Group, prob.
J0016-4056	Field, 100	β Pictoris, 62
J0032-4405	AB Doradus, 94	None
J0034-0706	β Pictoris, 85	β Pictoris, 63
J0109-5100	Field, 100	β Pictoris, 73
J0117-3403	Tucana–Horologium, 89	None
J0205-1159	Carina-Near, 95	Hyades, 71
J0219-1938	Columba, 99	AB Doradus, 80
J0230-0953	β Pictoris, 96	AB Doradus, 41
J0408-1450	β Pictoris, 72	AB Doradus, 72
J0559-1404	Field, 100	AB Doradus, 64
J0624-4521	Field, 97	Argus, 62
J0859-1949	β Pictoris, 84	Argus, 67
J0928-1603	Carina-Near, 92	Carina-Near, 53
J1018-2909	β Pictoris, 86	None
J1045-0149	Carina-Near, 97	None
J1047-1815	Carina-Near, 97	None
J1126-5003	Carina-Near, 94	None
J1326-2729	Carina-Near, 81	None
J1425-3650	AB Doradus, 100	None
J1520-4422	Carina-Near, 93	None
J1753-6559	AB Doradus, 92	Argus, 95
J1928-4356	AB Doradus, 98	AB Doradus, 54
J1936-5502	Field, 100	AB Doradus, 60
J2026-2943	Field, 100	AB Doradus, 55
J2130-0845	Carina-Near, 85	AB Doradus, 79
J2204-5646	Carina-Near, 98	None
J2206-4217	AB Doradus, 96	None
J2255-0034	Field, 100	AB Doradus, 93
J2351-2537	Field, 100	Hyades, 84

spectral type variations. We expect the number of sub-stellar objects with known parallaxes to grow and the availability of statistically significant samples will allow us to strengthen the constraints on models and to search for fundamental calibrators.

Concurrent with this contribution there will be the second data release of the *Gaia* mission which will have parallaxes and proper motions for 1.3 billion sources and positions for a further 200 million.[5] For objects later than L0, the number in the *Gaia* results will be quite modest, 500–1500 L0 to L5 dwarfs and 100–300 L5 to L9 dwarfs and less than 10 T dwarfs (Sarro et al. 2013; Smart et al. 2017b; Theissen 2018). In the first *Gaia* data release, only 38 PAR-SEC objects were found and we do not expect there to be many more with parallaxes and proper motions in the second data release.

The PARSEC objects are at the magnitude limit of *Gaia* $G = 21.3$ (Gaia Collaboration et al. 2016a), so these results will provide a first check on the *Gaia* results (Smart et al. 2017b). The PAR-SEC observations of objects in the *Gaia* catalogue will more than double the temporal baseline allowing the search for unresolved companions at significantly longer orbits. The PARSEC results for the objects fainter than the *Gaia* limit will remain valuable complementing that mission for science at the stellar and brown dwarf boundary. Finally, in the case of fainter targets, the *Gaia* astrometry of the brighter anonymous field stars will also allow us to improve reductions using small field astrometry especially in the estimation

[5]www.cosmos.esa.int/web/gaia/dr2

of the correction from relative to absolute parallax that remains a constant floor to what can be achieved with small field astrometry.

REFERENCES

Ahn C. P. et al., 2014, ApJS, 211, 17
Allard F., Homeier D., Freytag B., 2012, Phil. Trans. R. Soc. A, 370, 2765
Allers K. N., Liu M. C., 2013, ApJ, 772, 79
Andrei A. H. et al., 2011, AJ, 141, 54
Baade D. et al., 1999, The Messenger, 95, 15
Bardalez Gagliuffi D. C. et al., 2014, ApJ, 794, 143

Bayo A., Rodrigo C., Barrado Y Navascués D., Solano E., Gutiérrez R., Morales-Calderón M., Allard F., 2008, A&A, 492, 277

Becklin E. E., Zuckerman B., 1988, Nature, 336, 656

Blake C. H., Charbonneau D., White R. J., 2010, ApJ, 723, 684

Bouy H., Brandner W., Martín E. L., Delfosse X., Allard F., Basri G., 2003, AJ, 126, 1526

Bouy H., Martín E. L., Brandner W., Bouvier J., 2005, AJ, 129, 511

Burgasser A. J. et al., 1999, ApJ, 522, L65

Burgasser A. J. et al., 2000a, AJ, 120, 1100

Burgasser A. J. et al., 2000b, ApJ, 531, L57

Burgasser A. J. et al., 2002, ApJ, 564, 421

Burgasser A. J. et al., 2003c, ApJ, 592, 1186

Burgasser A. J. et al., 2015, ApJS, 220, 18

Burgasser A. J., 2004, ApJ, 614, L73

Burgasser A. J., McElwain M. W., Kirkpatrick J. D., 2003a, AJ, 126, 2487

Burgasser A. J., Kirkpatrick J. D., Reid I. N., Brown M. E., Miskey C. L., Gizis J. E., 2003b, ApJ, 586, 512

Burgasser A. J., Kirkpatrick J. D., Cruz K. L., Reid I. N., Leggett S. K., Liebert J., Burrows A., Brown M. E., 2006a, ApJS, 166, 585

Burgasser A. J., Burrows A., Kirkpatrick J. D., 2006b, ApJ, 639, 1095

Burgasser A. J., Looper D. L., Kirkpatrick J. D., Cruz K. L., Swift B. J., 2008, ApJ, 674, 451

Burrows A., Heng K., Nampaisarn T., 2011, ApJ, 736, 47

Chabrier G., Baraffe I., Leconte J., Gallardo J., Barman T., 2009, in Stempels E., ed., AIP Conf. Proc. Vol. 1094, 15th Cambridge Workshop on Cool Stars, Stellar Systems, and the Sun. Am. Inst. Phys., New York , p. 102

Chambers K. C. et al., 2016, preprint (arXiv:1612.05560)

Chiu K., Fan X., Leggett S. K., Golimowski D. A., Zheng W., Geballe T. R., Schneider D. P., Brinkmann J., 2006, AJ, 131, 2722

Cioni M.-R. L. et al., 2011, A&A, 527, A116

Cruz K. L. et al., 2007, AJ, 133, 439

Cruz K. L., Reid I. N., Liebert J., Kirkpatrick J. D., Lowrance P. J., 2003, AJ, 126, 2421

Cruz K. L., Burgasser A. J., Reid I. N., Liebert J., 2004, ApJ, 604, L61

Cruz K. L., Kirkpatrick J. D., Burgasser A. J., 2009, AJ, 137, 3345

Dahn C. C. et al., 2002, AJ, 124, 1170

Delfosse X. et al., 1997, A&A, 327, L25

Delfosse X., Tinney C. G., Forveille T., Epchtein N., Borsenberger J., Fouqué P., Kimeswenger S., Tiphène D., 1999, A&AS, 135, 41

Dieterich S. B., Henry T. J., Jao W.-C., Winters J. G., Hosey A. D., Riedel A. R., Subasavage J. P., 2014, AJ, 147, 94

Ducourant C., Teixeira R., Hambly N. C., Oppenheimer B. R., Hawkins M. R. S., Rapaport M., Modolo J., Lecampion J. F., 2007, A&A, 470, 387

Dupuy T. J., Kraus A. L., 2013, Science, 341, 1492

Dupuy T. J., Liu M. C., 2012, ApJS, 201, 19

Dupuy T. J., Liu M. C., 2017, ApJS, 231, 15

EROS Collaboration et al., 1999, A&A, 351, L5

ESA, 1997, ESA SP-1200: The *Hipparcos* and Tycho catalogues. Astrometric and photometric star catalogues derived from the ESA *Hipparcos* Space Astrometry Mission. ESA, Noordwijk

Faherty J. K. et al., 2012, ApJ, 752, 56

Faherty J. K. et al., 2016, ApJS, 225, 10

Faherty J. K., Burgasser A. J., Cruz K. L., Shara M. M., Walter F. M., Gelino C. R., 2009, AJ, 137, 1

Fan X. et al., 2000, AJ, 119, 928

Folkes S. L., Pinfield D. J., Kendall T. R., Jones H. R. A., 2007, MNRAS, 378, 901

Francis C., Anderson E., 2009, New Astron., 14, 615

Gagné J. et al., 2015a, ApJS, 219, 33

Gagné J. et al., 2018, ApJ, 856, 23

Gagné J., Lafrenière D., Doyon R., Malo L., Artigau É., 2014, ApJ, 783, 121

Gagné J., Lafrenière D., Doyon R., Malo L., Artigau É., 2015b, ApJ, 798, 73

Gaia Collaboration et al., 2016a, A&A, 595, A1

Gaia Collaboration et al., 2016b, A&A, 595, A2

Gálvez-Ortiz M. C. et al., 2010, MNRAS, 409, 552

Geballe T. R. et al., 2002, ApJ, 564, 466

Gelino C. R., Burgasser A. J., 2010, AJ, 140, 110

Gizis J. E., 2002, ApJ, 575, 484

Gizis J. E., Kirkpatrick J. D., Wilson J. C., 2001, AJ, 121, 2185

Golimowski D. A. et al., 2004, AJ, 128, 1733

Guenther E. W., Wuchterl G., 2003, A&A, 401, 677

Hawley S. L. et al., 2002, AJ, 123, 3409

Henry T. J., Jao W.-C., Subasavage J. P., Beaulieu T. D., Ianna P. A., Costa E., Méndez R. A., 2006, AJ, 132, 2360

Jameson R. F., Casewell S. L., Bannister N. P., Lodieu N., Keresztes K., Dobbie P. D., Hodgkin S. T., 2008, MNRAS, 384, 1399

Johnson D. R. H., Soderblom D. R., 1987, AJ, 93, 864

Kendall T. R. et al., 2007, A&A, 466, 1059

Kendall T. R., Mauron N., Azzopardi M., Gigoyan K., 2003, A&A, 403, 929

Kendall T. R., Delfosse X., Martín E. L., Forveille T., 2004, A&A, 416, L17

Kirkpatrick J. D. et al., 1999, ApJ, 519, 802

Kirkpatrick J. D. et al., 2000, AJ, 120, 447

Kirkpatrick J. D. et al., 2008, ApJ, 689, 1295

Kirkpatrick J. D., Dahn C. C., Monet D. G., Reid I. N., Gizis J. E., Liebert J., Burgasser A. J., 2001, AJ, 121, 3235

Knapp G. R. et al., 2004, AJ, 127, 3553

Latham D. W., Stefanik R. P., Mazeh T., Mayor M., Burki G., 1989, Nature, 339, 38

Laureijs R. J., Duvet L., Escudero Sanz I., Gondoin P., Lumb D. H., Oosterbroek T., Saavedra Criado G., 2010, in Oschmann J. M. Jr., Clampin M. C., MacEwen H. A., eds, Proc. SPIE Conf. Ser. Vol. 7731, Space Telescopes and Instrumentation 2010: Optical, Infrared, and Millimeter Wave. SPIE, Bellingham, p. 77311H

Lawrence A. et al., 2007, MNRAS, 379, 1599

Leggett S. K. et al., 2000, ApJ, 536, L35

Lépine S., Hilton E. J., Mann A. W., Wilde M., Rojas-Ayala B., Cruz K. L., Gaidos E., 2013, AJ, 145, 102

Liebert J., Kirkpatrick J. D., Cruz K. L., Reid I. N., Burgasser A., Tinney C. G., Gizis J. E., 2003, AJ, 125, 343

Liu M. C., Dupuy T. J., Allers K. N., 2016, ApJ, 833, 96

Lodieu N., Scholz R.-D., McCaughrean M. J., 2002, A&A, 389, L20

Lodieu N., Scholz R.-D., McCaughrean M. J., Ibata R., Irwin M., Zinnecker H., 2005, A&A, 440, 1061

Looper D. L., Kirkpatrick J. D., Burgasser A. J., 2007, AJ, 134, 1162

Looper D. L., Gelino C. R., Burgasser A. J., Kirkpatrick J. D., 2008, ApJ, 685, 1183

LSST Science Collaboration et al., 2017, preprint (arXiv:1708.04058)

Mace G. N. et al., 2013, ApJS, 205, 6

Maíz Apellániz J., 2017, A&A, 608, L8

Malo L., Doyon R., Lafrenière D., Artigau É., Gagné J., Baron F., Riedel A., 2013, ApJ, 762, 88

Manjavacas E. et al., 2016, MNRAS, 455, 1341

Marocco F. et al., 2013, AJ, 146, 161

Martín E. L. et al., 2010, A&A, 517, A53

Martín E. L., Delfosse X., Basri G., Goldman B., Forveille T., Zapatero Osorio M. R., 1999, AJ, 118, 2466

Mason B. D., Wycoff G. L., Hartkopf W. I., Douglass G. G., Worley C. E., 2001, AJ, 122, 3466

McElwain M. W., Burgasser A. J., 2006, AJ, 132, 2074

McMahon R. G., Banerji M., Gonzalez E., Koposov S. E., Bejar V. J., Lodieu N., Rebolo R. VHS Collaboration, 2013, The Messenger, 154, 35

Mendez R. A., van Altena W. F., 1996, AJ, 112, 655

Miles-Páez P. A., Metchev S. A., Heinze A., Apai D., 2017, ApJ, 840, 83

Minniti D. et al., 2010, New A, 15, 433

Monet D. G., Dahn C. C., Vrba F. J., Harris H. C., Pier J. R., Luginbuhl C. B., Ables H. D., 1992, AJ, 103, 638

Paudel R. R., Gizis J. E., Mullan D. J., Schmidt S. J., Burgasser A. J., Williams P. K. G., Berger E., 2018, ApJ, 861, 76

Reid I. N., Kirkpatrick J. D., Gizis J. E., Dahn C. C., Monet D. G., Williams R. J., Liebert J., Burgasser A. J., 2000, AJ, 119, 369

Reid I. N., Lewitus E., Allen P. R., Cruz K. L., Burgasser A. J., 2006a, AJ, 132, 891

Reid I. N., Lewitus E., Burgasser A. J., Cruz K. L., 2006b, ApJ, 639, 1114

Reid I. N., Cruz K. L., Kirkpatrick J. D., Allen P. R., Mungall F., Liebert J., Lowrance P., Sweet A., 2008, AJ, 136, 1290

Reiners A., Basri G., 2009, ApJ, 705, 1416

Riedel A. R., Blunt S. C., Lambrides E. L., Rice E. L., Cruz K. L., Faherty J. K., 2017, AJ, 153, 95

Sahlmann J., Lazorenko P. F., Ségransan D., Martín E. L., Mayor M., Queloz D., Udry S., 2014, A&A, 565, A20

Sarro L. M., Berihuete A., Carrión C., Barrado D., Cruz P., Isasi Y., 2013, A&A, 550, A44

Schmidt S. J., West A. A., Hawley S. L., Pineda J. S., 2010, AJ, 139, 1808

Schneider D. P. et al., 2002, AJ, 123, 458

Schneider A. C., Cushing M. C., Kirkpatrick J. D., Mace G. N., Gelino C. R., Faherty J. K., Fajardo-Acosta S., Sheppard S. S., 2014, AJ, 147, 34

Scholz R.-D., Meusinger H., 2002, MNRAS, 336, L49

Scholz R.-D., McCaughrean M. J., Lodieu N., Kuhlbrodt B., 2003, A&A, 398, L29

Scholz R.-D., Lehmann I., Matute I., Zinnecker H., 2004, A&A, 425, 519

Schönrich R., Binney J., Dehnen W., 2010, MNRAS, 403, 1829

Seifahrt A., Mugrauer M., Wiese M., Neuhäuser R., Guenther E. W., 2005a, Astron. Nachr., 326, 974

Seifahrt A., Guenther E., Neuhäuser R., 2005b, A&A, 440, 967

Seifahrt A., Reiners A., Almaghrbi K. A. M., Basri G., 2010, A&A, 512, A37

Skrutskie M. F. et al., 2006, AJ, 131, 1163

Smart R. L. et al., 2013, MNRAS, 433, 2054

Smart R. L. et al., 2017a, MNRAS, 468, 3764

Smart R. L., Bucciarelli B., Lattanzi M. G., Massone G., Chiumiento G., 1999, A&A, 348, 653

Smart R. L., Marocco F., Caballero J. A., Jones H. R. A., Barrado D., Beamín J. C., Pinfield D. J., Sarro L. M., 2017b, MNRAS, 469, 401

Spergel D. et al., 2015, preprint (arXiv:1503.03757)

Stephens D. C., Leggett S. K., 2004, PASP, 116, 9

Theissen C. A., 2018, ApJ, 862, 173

Thompson M. A. et al., 2013, PASP, 125, 809

Tinney C. G., Burgasser A. J., Kirkpatrick J. D., 2003, AJ, 126, 975

Tinney C. G., Burgasser A. J., Kirkpatrick J. D., McElwain M. W., 2005, AJ, 130, 2326

van Leeuwen F., 2007, A&A, 474, 653

Vrba F. J. et al., 2004, AJ, 127, 2948

Wang Y. et al., 2018, PASP, 130, 064402

Weinberger A. J., Boss A. P., Keiser S. A., Anglada-Escudé G., Thompson I. B., Burley G., 2016, AJ, 152, 24

West A. A., Hawley S. L., Bochanski J. J., Covey K. R., Reid I. N., Dhital S., Hilton E. J., Masuda M., 2008, AJ, 135, 785

Wielen R., 1977, A&A, 60, 263

Wilson J. C., Kirkpatrick J. D., Gizis J. E., Skrutskie M. F., Monet D. G., Houck J. R., 2001, AJ, 122, 1989

Wilson J. C., Miller N. A., Gizis J. E., Skrutskie M. F., Houck J. R., Kirkpatrick J. D., Burgasser A. J., Monet D. G., 2003, in Martín E., ed., Proc. IAU Symp. 211, Brown Dwarfs, Hawaii, United States, p. 197

Zapatero Osorio M. R., Martín E. L., Béjar V. J. S., Bouy H., Deshpande R., Wainscoat R. J., 2007, ApJ, 666, 1205

Zhang Z. H., Homeier D., Pinfield D. J., Lodieu N., Jones H. R. A., Allard F., Pavlenko Y. V., 2017, MNRAS, 468, 261

This paper has been typeset from a TEX/LATEX file prepared by the author.